UDC 620.193:669.14

THERMODYNAMIC ASSESSMENT OF CHEMICAL AND ELECTROCHEMICAL STABILITY OF IRON SILICIDES

P.A. Nikolaychuk

Institut für Biochemie, Universität Greifswald,
Felix-Hausdorff-Straße 4, 17487 Greifswald, Germany. E-mail: npa@csu.ru

Recieved 06.02.2019

***Abstract**: The phase and chemical equilibria in the Fe – Si system at 298 K were considered. The comparison between the available thermodynamic information on the solid solubility of silicon in bcc-iron at low temperatures was performed with and without consideration of the α-phase long distance ordering. The standard Gibbs energy of formation for non-stoichiometric iron silicide was estimated. The possible maximum solid solubility of Si in bcc-Fe at 298 K was estimated. The thermodynamic activities of the components in this saturated solution were calculated. The state diagram of the Fe – Si – O system at 298 K was plotted and the characteristics of their invariant conditions were calculated. The solid solubility of Fe_2SiO_4 in Fe_3O_4 and of SiO_2 in Fe_2O_3 at 298 K was estimated. The activity – pH diagrams for the aqueous Fe (II) and Fe (III) species were constructed. The potential – pH diagram of the Fe – Si – H_2O system at 298 K, air pressure of 1 bar and activities of ions in solution, equal to 1 mol l^{-1} was plotted. Basic chemical and electrochemical equilibria in this system were considered. The thermodynamic analysis of chemical and electrochemical stability of the Fe – Si system alloys was performed.*

***Keywords**: Fe – Si system, iron silicides, phase equilibria, low temperature oxidation, chemical and electrochemical stability.*
DOI: 10.32737/2221-8688-2019-2-155-184

1. Introduction

Iron–silicon is a very important binary system. Reliable information on the thermodynamic properties and phase equilibriums in Fe – Si alloys is needed for calculation of the technological quantities for various metallurgical processes. Iron silicides are perspective materials, including metalloid conductors [1], semiconductors [2, 3] and amorphous materials [4], they are well-known for their unusual magnetic, optical and thermodynamic properties [5 – 7]. Iron-silicon alloys can be found in Earth's core [8], they are used in the technology as thin films [9] and nanowires [2, 10]. Moreover, many important ternary and multicomponent systems, including Fe - Si binary system, such as Ni – Fe – Si [11], Al – Fe – Si [12 – 14], Fe – Mn – Si [15, 16], Cu – Fe – Si [17, 18], Cr – Fe – Si [19], Fe – Zn – Si [20 – 22], Fe – Si – C [23 – 26], Fe – Si – O [27, 28], Fe – Si – B [29, 30], Al – Ca – Fe – Si [31] and others, are of great interest for the researchers. The Fe – Si system-based alloys and compounds can be used as corrosion-resistant materials and coatings. The experimental investigations of iron silicides corrosion properties are very intensive; it will be discussed further in the section 5. However, the theoretical research into the issue is also important scientific task. One of the methods to describe the oxidation of silicides both in oxygen-containing gaseous environments (chemical stability) and in water environments (electrochemical stability) is the thermodynamic modelling. The previous investigations of thermodynamic features of Fe – Si system corrosion and oxidation properties [32, 33] do not cover all possible chemical and electrochemical equilibria in the system. The purpose of this study is to revise previous studies and take into account all

uncounted thermodynamic properties. Unlike many other published papers devoted to thermodynamic modeling at higher temperatures, the present paper describes thermodynamic description of alloy oxidation processes of Fe – Si system at standard temperature only.

2. Phase and chemical equilibria in Fe – Si system at the temperature of 298 K.
2. 1. Comparison of previous thermodynamic descriptions

According to the Fe – Si phase diagram [34 – 35], there are a number of intermetallic phases in the systems Fe_3Si_7, $FeSi_2$, FeSi, Fe_5Si_3 and Fe_2Si. But only $FeSi_2$ and FeSi are thermodynamically stable at standard conditions. FeSi has a narrow homogeneity range [7, 34], from $FeSi_{0,961}$ to $FeSi_{1,\,033}$ which doesn't depend on temperature. Pure silicon is available in diamond modification (Strukturbericht symbol is A4), and the solid solubility of iron inside is negligibly small and can be ignored. Iron exists in face-centered cubic (fcc) and body-centered cubic (bcc) modifications, but only the bcc one is stable at 298 K, and it is called α-Fe. The solid solubility of Si in α-Fe is equal to approx. 25 atomic percent while silicon can form three types of solutions. The first one is the disordered phase where only short range ordering exist (α-phase, the Strukturbericht symbol is A2), two others have long range atomic ordering – α_2-phase, the Strukturbericht symbol is B2 and α_1-phase, the Strukturbericht symbol is DO_3. The crystallographic features and lattice parameters of these phases were described many times [36 – 38]. Additionally, a miscibility gap exists between α_2 and α_1 phases. The magnetic transformation, which occurs in α-phase, corresponds to elevated temperatures and inflicts no effect on Fe – Si system thermodynamic properties at standard temperature. The Gibbs energy of the magnetic ordering is considered in studies [26, 38] and taken into no account in the present study.

However, there is no single and clear opinion about phase boundaries between α, α_2 and α_1 phases at low temperatures. Experimental data [39 – 41] are available only for high temperatures, all studies, considering Fe – Si phase diagram [34 – 38], provide reliable information about phase boundaries at the temperature diagram exceeding 500º C. Note that attempts of thermodynamic extrapolation of phase diagram below 500ºC are often contradictory. Some studies [34, 36] indicate that $\alpha - \alpha_2 - \alpha_1$ transformations take place at silicon concentration in solutions slightly above 10 atomic percent. On the other hand, the authors of [38] provide relations between temperatures of phase transition from A2 phase to B2 (T_{A2-B2}) and from B2 phase to DO_3 (T_{B2-DO_3}) and mole fraction of silicon in solid solution (x) as follows:

$$T_{A2-B2} = x\cdot(1-x)\cdot(-4293{,}3\cdot(1-2x)^3 - 112{,}5\cdot(1-2x)^2 + 2515{,}2\cdot(1-2x) + 9825{,}6) \quad (1),$$

$$T_{B2-DO_3} = x\cdot(1-2x)\cdot(134\cdot(1-4x)^3 - 4291{,}1\cdot(1-4x)^2 - 2306{,}2\cdot(1-4x) + 12024) \quad (2),$$

where temperatures T_{A2-B2} and T_{B2-DO_3} are given in Kelvins, mole fraction x is dimensionless. These equations are written to fit the experimental data of [39], but they can be solved in relation to x at the transition temperatures set to 298 K, this solution gives x = 0,036 for A2 – B2 transition and x = 0,045 for B2 – DO_3 transition. Moreover, there is no information about the exact position of miscibility gap between α_2 and α_1 phases. And finally, authors of [42] declare that there is no B2 phase either at low temperatures!

As for thermodynamic assessment of ternary and multicomponent systems [12, 13, 15 – 18, 20, 22, 24, 25, 28 – 31], most researchers refer to thermodynamic information about Fe – Si binary system provided in few descriptions [23, 38, 43]. Additionally, the authors of [20] provide their own thermodynamic description of Fe – Si α-phase. All of these descriptions do not take into account long range ordering transformations in α-phase completely. The authors of [20, 43] simply ignore it; the authors of [23] consider only α_2-phase using

two-sub-lattice model [44] but provide the analytical expression for the excess Gibbs energy G^E [45] without considering α_2-phase; the authors of [38] give analytical expressions for the atomic ordering Gibbs energy for both α_2 and α_1 phases but also offer a single equation for the excess Gibbs energy for all types of solid solutions, without contribution of atomic ordering to it. All of these descriptions estimate FeSi as the stoichiometric phase, without considering its homogeneity range.

Since in all above-mentioned studies [20, 23, 38, 43] the thermodynamic properties of the solid solution are estimated, with due regard for all possible equilibriums with α-phase involved, especially in high-temperature region, values of the estimated parameters, provide minimal deviations from the calculated Fe – Si phase diagram from the experimental one, but these deviations are still significant when only one single equilibrium is taken into account.

However, when considering equilibriums taken separately, these deviations matter. To estimate maximum silicon solid solubility in α-Fe at 298 K, it is important to specify the equilibrium of α-phase with FeSi compound. Therefore the comparison between all available descriptions was performed in order to select one of them and thus ensure the best matching of calculated and experimental data on this single equilibrium. So, at temperatures below 820º C [34, 36] with Fe-rich side on Fe – Si system, the following reaction occurs between α-phase (bcc solid solution) and FeSi compound:

$$\mathrm{Fe}\ (\alpha) + \mathrm{Si}\ (\alpha) = \mathrm{FeSi} \qquad (3).$$

It can be described using the following equation:

$$\Delta_r G_T^o = -RT \cdot \ln K_p = -RT \cdot \ln \frac{1}{a_{\mathrm{Fe}(\alpha)} \cdot a_{\mathrm{Si}(\alpha)}} = RT \cdot \ln a_{\mathrm{Fe}(\alpha)} + RT \cdot \ln a_{\mathrm{Si}(\alpha)} \qquad (4),$$

where $\Delta_r G_T^o$ is the Gibbs energy change of reaction (3), J mol^{-1}, K_p is an equilibrium constant of this reaction, $R = 8{,}3144\ \mathrm{J\,mol^{-1}\,K^{-1}}$ is a universal gas constant, T is a temperature in Kelvins, $a_{\mathrm{Fe}(\alpha)}$ and $a_{\mathrm{Si}(\alpha)}$ are, respectively, thermodynamic activities of iron and silicon in α-phase (reference state – pure component with bcc lattice), which is in equilibrium with FeSi. Here and further in the text, unless otherwise agreed, all compounds, including silicides, oxides and silicates, are treated as pure substances, and their activities are set to unity. The analytical expressions of $a_{\mathrm{Fe}(\alpha)}$ and $a_{\mathrm{Si}(\alpha)}$ are linked with an expression for the excess Gibbs energy G^E of α-phase:

$$RT \cdot \ln a_{i(\alpha)} = RT \cdot \ln x_{i(\alpha)} + \mu_{i(\alpha)}^{\mathrm{E}} \qquad (5),$$

where $i(\alpha)$ denotes any α-phase component (Fe or Si), $x_{i(\alpha)}$ is the mole fraction of the component i and $\mu_{i(\alpha)}^{\mathrm{E}}$ is an excess chemical potential of the component that can be determined as the partial derivative of excess Gibbs energy G^E with respect to the number of moles of this component [45]. Thus, the analytical expression of $G_\alpha^{\mathrm{E}} = \mathrm{f}\,(x_{\mathrm{Fe}(\alpha)}, x_{\mathrm{Si}(\alpha)}, T)$ is needed to solve equation (4).

In the paper [43], the following equations are proposed for the Gibbs energy change of reaction (3) and for the excessive Gibbs energy of α-phase:

$$\Delta_r G_T^o\ (3) = 27{,}572T - 123010,\ \mathrm{J\ mol^{-1}} \qquad (6),$$

$$G_\alpha^E = x(1-x) \cdot ((1-x) \cdot (7{,}95T - 129704) + x \cdot (136{,}82T - 297064)),\ \mathrm{J\ mol^{-1}} \qquad (7).$$

Here x denotes the silicon mole fraction in the solid solution.

The authors of [20] also use the equation (6) for Gibbs energy change of reaction (3); however, it offers the description of G_α^{E} according to Redlich-Kister power series [46]:

$$G_{\alpha}^{E} = x(1-x)\cdot((34{,}81T - 156900) + (1-2x)\cdot(-0{,}41T - 33470) + \\ + (1-2x)^2\cdot(-11{,}08T + 35780) + (1-2x)^3\cdot(-6{,}92T - 28800)),\ \text{J mol}^{-1} \quad (8).$$

Another set of parameters is proposed by the authors of the paper [38]. They consider the reaction of FeSi formation in the following form:

$$\text{Fe}\ (\gamma) + \text{Si}\ (\text{diamond}) = \text{FeSi} \quad (9),$$

and provide the value of Gibbs energy change in the reaction (9) by the equation

$$\Delta_r G_T^o\ (9) = 10{,}2906T - 86421{,}72,\ \text{J mol}^{-1} \quad (10).$$

Additionally, they consider reactions of phase transitions of iron and silicon:

$$\text{Fe}\ (\gamma) = \text{Fe}\ (\alpha) \quad (11),$$

$$\text{Si}\ (\text{diamond}) = \text{Si}\ (\alpha) \quad (12),$$

and provide the values of Gibbs energies of these transitions:

$$\Delta_r G_T^o\ (11) = \Delta_{tr} G_T^o\ (\text{Fe}_{\gamma\to\alpha}) = -6{,}4\cdot 10^{-4}T^2 - 8{,}282T + 1{,}15T\cdot\ln T + 1462{,}4,\ \text{J mol}^{-1} \quad (13),$$

$$\Delta_r G_T^o\ (12) = \Delta_{tr} G_T^o\ (\text{Si}_{\text{diamond}\to\alpha}) = -19{,}54T + 44350,\ \text{J mol}^{-1} \quad (14).$$

Obviously, the Gibbs energy of reaction (3) can be calculated according to Hess' law:

$$\Delta_r G_T^o\ (3) = \Delta_r G_T^o\ (9) - \Delta_r G_T^o\ (11) - \Delta_r G_T^o\ (12) \quad (15).$$

The equation for excess Gibbs energy G_{α}^{E} is also written according to Redlich-Kister formalism:

$$G_{\alpha}^{E} = x(1-x)\cdot((13{,}7306T - 129038) - 39244\cdot(1-2x)),\ \text{J mol}^{-1} \quad (16).$$

And, finally, the authors of [23] give another set of parameters. They consider formation of FeSi from the elements in their standard reference states at low temperatures:

$$\text{Fe}\ (\alpha) + \text{Si}\ (\text{diamond}) = \text{FeSi} \quad (17),$$

providing the value of Gibbs energy of reaction (17) by the equation

$$\Delta_r G_T^o\ (17) = 4{,}44T - 72761{,}2,\ \text{J mol}^{-1} \quad (18).$$

This time, the Gibbs energy of reaction (3) can be gained in the following way:

$$\Delta_r G_T^o\ (3) = \Delta_r G_T^o\ (17) - \Delta_r G_T^o\ (12) \quad (19),$$

But instead of using Gibbs energy change of reaction (12) offered in [38] and listed in the equation (14), the authors of [23] use the value, obtained from database [47]:

$$\Delta_r G_T^o\ (12) = \Delta_{tr} G_T^o\ (\text{Si}_{\text{diamond}\to\alpha}) = -22{,}5T + 47000,\ \text{J mol}^{-1} \quad (20).$$

And the excessive Gibbs energy G_{α}^{E} is presented in the following form:

$$G_{\alpha}^{E} = x(1-x)\cdot((46{,}48T - 111236) - 92352\cdot(1-2x) + 62240\cdot(1-2x)^2),\ \text{J mol}^{-1} \quad (21).$$

After substituting values of these parameters for the equation (4), only two variables remain in it: *T* and *x*. The solution of this equation provides the position of line on the Fe – Si phase diagram that corresponds to maximum silicon solid solubility. The solutions obtained with all of above-mentioned parameters sets as compared with values obtained from currently accepted Fe – Si phase diagram [34, 35], are presented **in Fig. 1**. As can be seen, the best convergence between the experimental and calculated lines is achieved when using parameters from the paper [43]. This allows to extrapolate this calculated equilibrium line down to the standard temperature. The estimated silicon maximum solid solubility at 298 corresponds to *x* = 0.262.

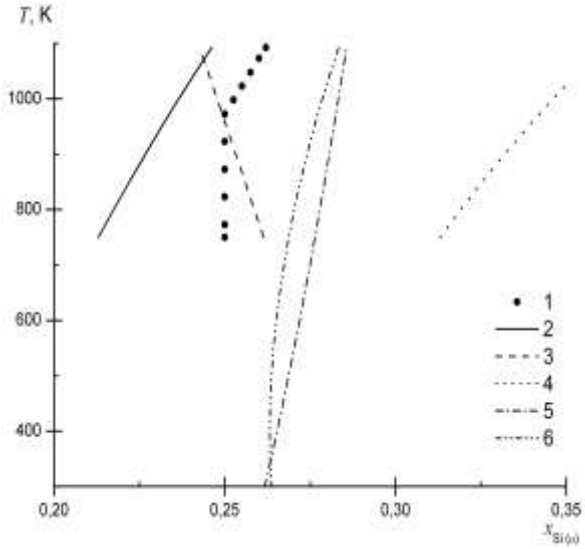

Figure 1. Maximum solid solubility of Si in α-Fe at various temperatures: *1* – experimental values, obtained from Fe – Si phase diagram [34, 35]; *2* – calculated according to data of [20] using equations (4), (6) and (8); *3* – calculated according to data of [23] using equations (4), (18), (20) and (21); *4* – calculated according to data of [38] using equations (4), (10), (13), (14) and (16); *5* – calculated according to data of [43] using equations (4), (6) and (7); *6* – calculated in present study using equations (7), (20), (25) and (27).

2.2. Considering the non-stoichiometry of FeSi compound

The next step is to extend this thermodynamic description by taking into account the non-stoichiometry of FeSi compound. There are no thermodynamic properties of non-stoichiometric FeSi in literature; therefore it is necessary to predict it. The authors of [48] notice that an approximate functional relationship exist between the reduced chemical potential of oxygen atoms in metal oxide and system oxidation degree: $\Delta_f G_T^o(\mathrm{Me}_{1/x}\mathrm{O}) = f(x)$. The assumption is made by in the paper [49] that similar relationship is valid not only for oxides but also for some other binary compounds with polar covalent bond (sulfides, carbides, nitrides, silicides, etc.). They derived the following interpolation formula for the Gibbs energy of binary compounds formation:

$$\Delta_f G_T^o(M_{a_x}A_{b_x}) = b_x \cdot \sum_{i=1}^{n}\left(\frac{\Delta_f G_T^o(M_{a_i}A_{b_i})}{b_i} \cdot \prod_{j\neq i}\frac{a_i \cdot (a_j \cdot b_x - a_x \cdot b_j)}{a_x \cdot (a_j \cdot b_i - a_i \cdot b_j)}\right) \qquad (22),$$

where n is a number of Gibbs energies of formation of binary compounds, accepted as a reliable initial data; $M_{a_i}A_{b_i}$ – formulae of these binary compounds (M – metal atom, A – more electronegative element atom,, a_i and b_i – indices for M and A atoms in compound, respectively); $M_{a_x}A_{b_x}$ – formula of the compound, Gibbs energy of formation of which is to be estimated, a_x and b_x – indices for the M and A atoms in it.

In spite of the fact that FeSi and $FeSi_2$ solely are stable compounds in the Fe – Si system at standard temperature, the information about the standard Gibbs energies of formation ($\Delta_f G_{298}^o$) for other iron silicides is also presented in literature. The data from [23, 38, 43, 50 – 57] are summarized **in table 1**.

Table 1. Standard Gibbs energies of formation of iron silicides (as referred to bcc Fe and diamond Si).

Compound / Reference	$\Delta_f G_{298}^o$, J mol^{-1}					
	Fe_3Si	Fe_2Si	Fe_5Si_3	FeSi	Fe_3Si_7	$FeSi_2$
[23]	–	–74421	–240500	–71438	–199231	–79038
[38]	–	–75414	–252822	–83355	–	–83764
[43]	–	–	–	–76266	–251934	–
[50]	–94765	–	–233643	–76587	–179307	–78447

[51]	–84592	–	–197639	–76579	–198495	–73291
[52]	–83740	–	–244510	–81600	–	–80390
[53]	–94605	–	–	–73223	–	–78357
[54]	–	–	–	–73765	–	–79660
[55]	–	–92064	–	–76028	–	–92593
[56]	–103200	–	–	–78600	–	–91800
[57]	–124656	–	–306841	–94056	–	–97762
*	–95850	–90180	–260340	–73180	–194900	–78360

As can be seen from Table 1, there is no convergence between the results given in various papers. The differences are often significant. Only the data for FeSi and $FeSi_2$ agree satisfactorily with one another. The most reliable information on standard Gibbs energies in the formation of these two silicides is obtained from the paper [54], because it was determined within the temperature range of $10\ \text{K} \le T \le 400\ \text{K}$ by means of adiabatic low-temperature calorimetry, while the data from some other papers involve extrapolations of thermodynamic properties from high-temperature region down to the standard temperature. From all studies containing dependencies of $\Delta_f G_T^o\ (\text{FeSi, FeSi}_2) = f(T)$ [23, 38, 50, 52, 53, 55, 57] only those from the study [53] closely match values from the paper [54]. In this case, the decision is made to use only data for FeSi and $FeSi_2$ from [53] when estimating the non-stoichiometric $FeSi_x$ with unknown thermodynamic properties. The values in [53] are tabulated in temperature range of $298\ \text{K} \le T \le 1200\ \text{K}$, and the approximation of them provides the following equations:

$$\Delta_f G_T^o\ (\text{FeSi}) = 0{,}0051T^2 - 2{,}8429T - 72785,\ \text{J mol}^{-1} \quad (23),$$

$$\Delta_f G_T^o\ (\text{FeSi}_2) = 0{,}0072T^2 + 4{,}4465T - 80321,\ \text{J mol}^{-1} \quad (24).$$

Substituting equations (23) and (24) for the equation (22) leads to the following equation for the Gibbs energy of formation of $FeSi_x$ phase:

$$\Delta_f G_T^o\ (\text{FeSi}_x) = x^2 \cdot (-0{,}0015T^2 + 5{,}06615T + 32624{,}5) + x \cdot (0{,}0066T^2 - 7{,}90905T - 105409{,}5),\ \text{J mol}^{-1} \quad (25).$$

Here x is an index in formula $FeSi_x$. In order to verify formula (25), the values of $\Delta_f G_{298}^o$ for all iron silicides are estimated in line with the above. They are shown in Table 1 in a column, marked by * and agree more or less satisfactorily with values presented in literature. Thus, this formula can be used for further calculations. It gives the following results at standard temperature: $\Delta_f G_{298}^o(\text{FeSi}_{0,961}) = -71600\ \text{J mol}^{-1}$ and $\Delta_f G_{298}^o(\text{FeSi}_{1,033}) = -74430\ \text{J mol}^{-1}$.

Now, the equations (3) and (4) can be replaced with the following ones:

$$\text{Fe}\ (\alpha) + 0{,}961\ \text{Si}\ (\alpha) = \text{FeSi}_{0,961} \quad (26).$$

$$\Delta_r G_T^o = -RT \cdot \ln \frac{1}{a_{\text{Fe}(\alpha)} \cdot a_{\text{Si}(\alpha)}^{0,961}} = RT \cdot \ln a_{\text{Fe}(\alpha)} + 0{,}961RT \cdot \ln a_{\text{Si}(\alpha)} \quad (27).$$

The Gibbs energy of formation of $FeSi_{0,961}$ obtained by setting x = 0,961 in the equation (25), however, refers to standard element reference states:

$$\text{Fe}\ (\alpha) + 0{,}961\ \text{Si}\ (\text{diamond}) = \text{FeSi}_{0,961} \quad (28),$$

And have to be combined with the reaction (12) according to Hess' law:

$$\Delta_r G_T^o\ (26) = \Delta_r G_T^o\ (28) - 0{,}961 \cdot \Delta_r G_T^o\ (12) \quad (29).$$

The expression of silicon Gibbs energy of transition in the reaction (12) is taken from the

equation (20), and previously chosen expression for excess Gibbs energy G^{E}_{α} from [43] (equation (7)) is used. The result of solving equation (27) is also shown in Fig. 1 (line *6*) and is very good compatible with values calculated without considering $FeSi_x$ non-stoichiometry (line *5*) and experimental phase diagram (line *1*). The estimated silicon maximum solid solubility at 298 K corresponds to x = 0,264, the activities of this "saturated" solid solution components are equal to $a_{Fe(\alpha)} = 0{,}114$ and $a_{Si(\alpha)} = 7{,}2 \cdot 10^{-20}$ which means essential negative deviations from ideal behavior.

2.3. Considering sub-silicide "Fe_3Si" and α-phase ordering

Also, an attempt is made to take into account atomic ordering in α-phase. But, unlike previous descriptions [23, 38], entirely different way is chosen. It is well known [36 – 38] that α_1-phase where full ordering occurs corresponds to alloy composition of $Fe_{0,75}Si_{0,25}$. Since the line of maximum silicon solid solubility in α-Fe, depicted in experimental Fe – Si phase diagram [34, 35] stands exactly on this alloy composition at low temperatures, it is possible to treat this fully ordered α_1-phase as the independent compound "Fe_3Si". There are several evidences in literature [4, 9, 16, 20, 23, 30, 36, 55, 56, 58 – 60] that consider Fe_3Si as low-temperature sub-silicide, moreover, even its standard Gibbs energy of formation is estimated in [50 – 53, 56, 57].

Usually, if the temperature is fixed, the next sequence of phase transitions is observed, when moving at the Fe-rich side of Fe – Si phase diagram in the direction of silicon concentration increase: α | α2 | α2 + α1 | α1 | α1 + FeSi0,961 and so on. However, if guided by authors' premise [42] that there is no α_2-phase at low temperatures, the sequence of phase transitions reduces to α | α_1 | α_1 + $FeSi_{0,961}$. When fully ordered α_1-phase is treated as the independent compound "Fe_3Si", the α_1 phase region can be described as the mixture of disordered α-phase and "Fe_3Si". Then the sequence of phase transitions becomes as follows: α | α + "Fe_3Si" | "Fe_3Si" + $FeSi_{0,961}$. This assumption is certainly a simplification but it allows avoiding addition of special parameters in the equations for the α-phase Gibbs energies to describe its ordering, as it was done in the paper [23, 38].

Instead of equations (3) and (4) describing the line of silicon maximum solid solubility in α-Fe, the next ones can be written now:

$$3\ \mathrm{Fe}\ (\alpha) + \mathrm{Si}\ (\alpha) = \text{"}Fe_3Si\text{"} \qquad (30).$$

$$\Delta_r G^o_T = -RT \cdot \ln \frac{1}{a^3_{Fe(\alpha)} \cdot a_{Si(\alpha)}} = 3RT \cdot \ln a_{Fe(\alpha)} + RT \cdot \ln a_{Si(\alpha)} \qquad (31).$$

Again the comparison between all available thermodynamic data for α-phase [20, 23, 38, 43] is made in order to choose the one that provides better description of this equilibrium. The procedure is similar to the one described in section 2. 1., and thus the calculations are omitted. It reveals that parameters from paper [23] are the best choice at this time. They are used to extrapolate equilibrium (30) down to the temperature of 298 K. The estimated silicon maximum solid solubility at 298 K corresponds to x = 0,112, the activities of solid solution components are equal to $a_{Fe(\alpha)} = 0{,}473$ and $a_{Si(\alpha)} = 5{,}5 \cdot 10^{-20}$, and deviations of this solution from ideal behavior are negative.

3. The chemical stability of iron silicides

3.1. Phase and chemical equilibriums in Fe – Si – O system at a temperature of 298 K

The chemical stability of an alloy or a compound is the ability to resist the chemical influence of natural environment, particularly, the oxidation by atmospheric oxygen [61, 62].

The thermodynamic features of Fe – Si system chemical stability can be clearly described by plotting Fe – Si – O system' state diagram and considering equilibriums in this system. But prior to plotting a diagram, the primary information about possible oxides in binary Fe – O and Si – O [34] systems, as well as about possible ternary compounds [63], must be taken into consideration.

Note that just one stable oxide – SiO_2 – exists in Si – O system. There are also many values of its Gibbs energy of formation available in literature [50 – 53]. However, since electrochemical formation of silicon dioxide is to be considered (see section 4), the value is chosen in line with experimentally determined potential of the silicon electrode [64]:

$$SiO_2 + 4H^+ + 4e^- = Si\,(diamond) + 2H_2O;\ \varphi^o_{298} = -0{,}857\,V \qquad (32),$$

which leads to the following equation:

$$Si\,(diamond) + O_2 = SiO_2;\ \Delta_r G^o_{298} = -805067\ J\ mol^{-1} \qquad (33).$$

In the system Fe – O at 25˚C two oxides are stable - Fe_3O_4 and Fe_2O_3 [34, 35]. In spite of the fact that standard Gibbs energy of formation of the iron monoxide FeO is negative ($\Delta_f G^o_{298}(FeO) = -244300\ ^{J}/_{mol}$ according to [51]), it is thermodynamically unstable at standard a temperature [62, 65] because it is decomposed spontaneously according to the reaction

$$4\ FeO = Fe\,(\alpha) + Fe_3O_4;\ \Delta_r G^o_{298} = -36960\,J\ mol^{-1} \qquad (34).$$

It is known [65] that some mixed metal oxides exist contain Fe O_2 layers. They are, for example, Ba_2FeO_4 and $SrFe_2O_4$ which can be introduced as $2BaO \cdot FeO_2$ and $2SrO \cdot FeO_2$ respectively. Moreover, the formation of ferrate-ions is possible in highly oxidized environments [65] and the electrochemical oxidation of Fe^{+3} state to Fe^{+6} one cannot proceed it in one step, because iron cannot lose three electrons at once [66]. Therefore, an intermediate Fe^{+4} aqueous state species probably exist in the solution. However, in the literature there is no available thermodynamic information about any solid or aqueous iron (IV) species, and at the present time there is no possibility to involve them into the thermodynamic modelling.

Information about thermodynamic functions of the iron oxides [50 – 53, 67, 68] is listed **in Table 2.**

Table 2. Standard Gibbs energies of formation of iron oxides (as referred to bcc Fe and gaseous O_2).

Reference / Compound	$\Delta_f G^o_{298}$, J mol^{-1}					
	[50]	[51]	[52]	[53]	[67]	[68]
Fe_3O_4	–1026182	–1014163	–1019112	–1015391	–1017438	–1007561
Fe_2O_3	–743800	–740337	–741613	–742413	–743523	–739991

A single ternary compound is available in Fe – Si – O system at a standard temperature and pressure, it is iron orthosilicate (or fayalite) Fe_2SiO_4 [63]. Another compound, ferrosilite $FeSiO_3$, is formed only at elevated temperatures or very high pressures [28]. Fayalite is available in two forms: α-Fe_2SiO_4 which has olivine crystal structure and γ-Fe_2SiO_4 with its spinel crystal structure [69, 70]. Note that just α-Fe_2SiO_4 is thermodynamically stable under standard conditions. The values of standard Gibbs energies of formation of α-Fe_2SiO_4 [28, 50 – 53, 69, 71, 72] are summarized **in Table 3.**

Table 3. Standard Gibbs energies of formation of iron silicate Fe_2SiO_4 (referred to bcc Fe, diamond Si and gaseous O_2).

Reference	[28]	[50]	[51]	[52]
$\Delta_f G^o_{298}$, J mol^{-1}	–1378035	–1375934	–1377004	–1347064
Reference	[53]	[69]	[71]	[72]
$\Delta_f G^o_{298}$, J mol^{-1}	–1380890	–1313750	–1379160	–1379188

In addition to iron silicates with well-known composition and structure, there are notifications [73, 74] that some silicates have unknown and complex composition and structure. One of the possible explanations of the fact is related to the ability of Fe_3O_4 to form a solid solution with Fe_2SiO_4, observed by the authors of [75 – 77]. Moreover, they observed a solid solubility of SiO_2 in Fe_2O_3. The information about solid solubility of these compounds at various temperatures [77] is **shown in Table 4**.

Table 4. The experimentally measured [77] solid solubility of Fe_3O_4 in Fe_2SiO_4 and SiO_2 in Fe_2O_3 at various temperatures.

System Fe_3O_4 – Fe_2SiO_4			System SiO_2 – Fe_2O_3		
Temperature, K	Solid solubility in		Temperature, K	Solid solubility in	
	mass %	atomic %		mass %	atomic %
1073	20.2	19.9	1073	7.7	18.2
1173	26.2	20.5	1173	9.3	21.4
1273	31.7	24.7	1273	10.9	24.5

The estimation of maximum solid solubility at 298 K is performed using thermodynamic modeling. The equilibrium between pure Fe_3O_4 (magnetite) and its solid solution in fayalite

$$Fe_3O_4\ (\text{magnetite}) = Fe_3O_4[\text{in } Fe_2SiO_4] \quad (35)$$

can be characterized with the equality of chemical potentials (μ) of Fe_3O_4 in both phases [45]:

$$\mu_{Fe_3O_4\ (\text{magnetite})} = \mu_{Fe_3O_4[\text{in } Fe_2SiO_4]} \quad (36).$$

Since magnetite is treated as pure substance under standard conditions, its chemical potential equals to the standard chemical potential

$$\mu_{Fe_3O_4\ (\text{magnetite})} = \mu^{o}_{Fe_3O_4\ (\text{magnetite})} \quad (37).$$

and chemical potential of Fe_3O_4 in the solution is presented by the sum of three terms:

$$\mu_{Fe_3O_4[\text{in } Fe_2SiO_4]} = \mu^{o}_{Fe_3O_4[\text{in } Fe_2SiO_4]} + RT \cdot \ln x_{Fe_3O_4[\text{in } Fe_2SiO_4]} + \mu^{E}_{Fe_3O_4[\text{in } Fe_2SiO_4]} \quad (38),$$

where $\mu^{o}_{Fe_3O_4[\text{in } Fe_2SiO_4]}$ is standard chemical potential of Fe_3O_4, referred to the lattice of solvent compound, Fe_2SiO_4; $\mu^{E}_{Fe_3O_4[\text{in } Fe_2SiO_4]}$ is its excess chemical potential and $x_{Fe_3O_4[\text{in } Fe_2SiO_4]}$ is the mole fractions of Fe_3O_4 corresponding to maximum solubility at a temperature *T*. The difference between standard chemical potentials of Fe_3O_4 in the magnetite lattice and in the lattice of solid solution is equal to molar Gibbs energy of transition of Fe_3O_4 from pure component to solution:

$$\Delta_{tr}G^{o}_{T}(Fe_3O_4\ (\text{magnetite}) \rightarrow Fe_3O_4[\text{in } Fe_2SiO_4]) = \mu^{o}_{Fe_3O_4[\text{in } Fe_2SiO_4]} - \mu^{o}_{Fe_3O_4\ (\text{magnetite})} \quad (39),$$

$$\Delta_{tr}G^{o}_{T}(Fe_3O_4\ (\text{magnetite}) \rightarrow Fe_3O_4[\text{in } Fe_2SiO_4]) = \Delta_{tr}H^{o}_{T} - T \cdot \Delta_{tr}S^{o}_{T} \quad (40).$$

Only the simplest thermodynamic models with minimal number of parameters can be employed to describe the excessive chemical potentials of solution components. This is

explained as being due to the lack of experimental data. The strictly regular solution model [78] is used following which:

$$\mu^{\mathrm{E}}_{\mathrm{Fe_3O_4[in\ Fe_2SiO_4]}} = (1 - x_{\mathrm{Fe_3O_4[in\ Fe_2SiO_4]}})^2 \cdot L_{\mathrm{Fe_3O_4,\ Fe_2SiO_4}} \quad (41).$$

where $L_{\mathrm{Fe_3O_4,\ Fe_2SiO_4}}$ is the energy of mixing the compounds in the solution, which isn't depend on temperature.

Substituting equations (37) through (41) for the equation (36) gives the following expression:

$$\Delta_{tr}H^{\mathrm{o}}_T - T \cdot \Delta_{tr}S^{\mathrm{o}}_T + RT \cdot \ln\, x_{\mathrm{Fe_3O_4[in\ Fe_2SiO_4]}} + (1 - x_{\mathrm{Fe_3O_4[in\ Fe_2SiO_4]}})^2 \cdot L_{\mathrm{Fe_3O_4,\ Fe_2SiO_4}} = 0 \quad (42).$$

Substituting data on T and $x_{\mathrm{Fe_3O_4[in\ Fe_2SiO_4]}}$ from Table 4 for the equation (42) provides the system of three linear equations with three variables. This system is solved according to Cramer's method [79]. As a result, values of the parameters are estimated as follows:

$$\Delta_{tr}G^{\mathrm{o}}_T(\mathrm{Fe_3O_4\,(magnetite) \rightarrow Fe_3O_4[in\ Fe_2SiO_4]}) = 0{,}235T - 1523,\ \mathrm{J\ mol^{-1}} \quad (43),$$

$$L_{\mathrm{Fe_3O_4,\ Fe_2SiO_4}} = 25216\ \mathrm{J\ mol^{-1}} \quad (44).$$

Then, in keeping with calculated values of parameters, the equation (42) can be solved according to $x_{\mathrm{Fe_3O_4[in\ Fe_2SiO_4]}}$ at a temperature T = 298 K. The calculated solid solubility of Fe_3O_4 in Fe_2SiO_4 at a standard temperature is $x_{\mathrm{Fe_3O_4[in\ Fe_2SiO_4]}} = 6{,}85 \cdot 10^{-5}$. Activities of solid solution components (reference state – pure component with fayalite lattice) are $a_{\mathrm{Fe_3O_4}} = 0{,}00233$ and $a_{\mathrm{Fe_2SiO_4}} \approx 1$.

The equilibrium between pure SiO_2 (quartz) and its solid solution in hematite

$$\mathrm{SiO_2\ (quartz) = SiO_2[in\ Fe_2O_3]} \quad (45)$$

can be described similarly to the preceeding one. The parameters are the molar Gibbs energy of phase transition of SiO_2 obtained from the lattice of pure compound (quartz) to the lattice of solution (hematite)

$$\Delta_{tr}G^{\mathrm{o}}_T(\mathrm{SiO_2\,(quartz) \rightarrow SiO_2[in\ Fe_2O_3]}) = \Delta_{tr}H^{\mathrm{o}}_T - T \cdot \Delta_{tr}S^{\mathrm{o}}_T \quad (46)$$

and the energy of mixing in strictly regular solution of SiO_2 and Fe_2O_3

$$\mu^{\mathrm{E}}_{\mathrm{SiO_2[in\ Fe_2O_3]}} = (1 - x_{\mathrm{SiO_2[in\ Fe_2O_3]}})^2 \cdot L_{\mathrm{SiO_2,\ Fe_2O_3}} \quad (47).$$

The resulting equation for thermodynamic calculations is similar to equation (42):

$$\Delta_{tr}H^{\mathrm{o}}_T - T \cdot \Delta_{tr}S^{\mathrm{o}}_T + RT \cdot \ln\, x_{\mathrm{SiO_2[in\ Fe_2O_3]}} + (1 - x_{\mathrm{SiO_2[in\ Fe_2O_3]}})^2 \cdot L_{\mathrm{SiO_2,\ Fe_2O_3}} = 0 \quad (48).$$

The results of solving equation (48) are the following:

$$\Delta_{tr}G^{\mathrm{o}}_T(\mathrm{SiO_2\,(quartz) \rightarrow SiO_2[in\ Fe_2O_3]}) = 2{,}621T + 6557,\ \mathrm{J\ mol^{-1}} \quad (49),$$

$$L_{\mathrm{SiO_2,\ Fe_2O_3}} = 8740\ \mathrm{J\ mol^{-1}} \quad (50).$$

The calculated solid solubility of SiO_2 in Fe_2O_3 at a standard temperature is $x_{\mathrm{SiO_2[in\ Fe_2O_3]}} = 1{,}54 \cdot 10^{-3}$. Activities of solid solution components (reference state – pure component with hematite lattice) are $a_{\mathrm{SiO_2}} = 0{,}0541$ and $a_{\mathrm{Fe_2O_3}} = 0{,}998$.

Both solid solutions reveal small positive deviations from ideal behavior. Calculated solid solubility at a standard temperature in both cases is vanishingly small. It inflicts no effect on crystal structure and composition of iron silicate.

3.2. The Fe – Si – O system state diagram

The method of plotting and describing three-component state diagrams for metal-oxygen-containing systems was developed in [61, 62]. The Diagram consists of two ordinary orthogonal axes. The abscissa is the mole fraction of one metal compound in binary

system; in the present study abscissa is presented by silicon mole fraction x_{Si}, assuming $x_{Fe} = 1 - x_{Si}$. The ordinate is presented by system oxidation degree (y) which is the quantity of moles of atomic oxygen in the system, corresponding to the one mole of metallic compounds; in present study it is determined as

$$y = \frac{n_O}{n_{Fe} + n_{Si}} \qquad (51).$$

The Diagram is plotted at fixed temperature and pressure. According to Gibbs' phase rule [45], when these two variables are fixed, maximum of three phases can coexist in three-component system. Any single compound (one-phase region) is described by any vertex within the diagram, a two-phase region is characterized by any tie-line between two nearest vertices, a three-phase region is depicted by any triangle and it corresponds to invariant system condition. Crossing tie-lines is not allowed because the point of their intersection would correspond to four-phase region which is impossible. Any phase of variable composition is noted by line; any triangle containing this line and filled with dotted lines corresponds to monovariant system condition.

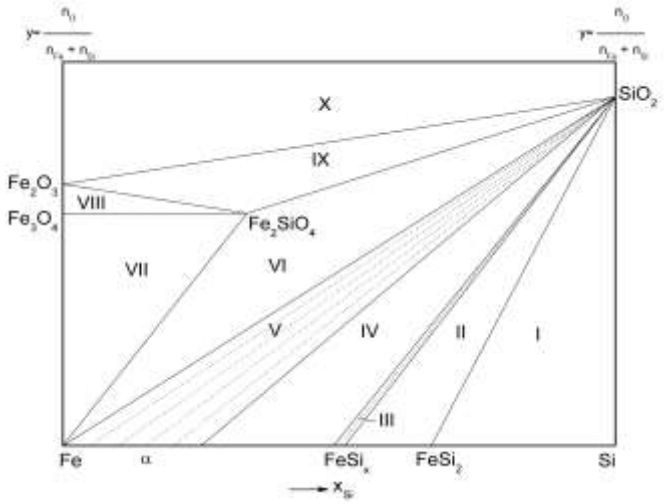

Figure 2. The Fe – Si – O state diagram at 298 K without consideration of "Fe_3 Si" drawn up according to the reference data

Thus, this kind of state diagram has the same functionality as does the ordinary triangle phase diagrams (which, for example, are plotted for some Metal – Si – O systems by the authors of [80]), but are easier to plot and examine.While any Fe – Si system compound is oxidizing, all equilibriums with oxygen (from thermodynamic point of view) take place in multiple stages, one after another. Since the chemical affinity of silicon to oxygen is much higher than that of iron [61], silicon from iron silicides has to be oxidized in the first order, and the consecutive formation of phases increasingly richer in iron has to be observed.

Along with this, the equilibrium oxygen pressure rises from the previous stage to the next one. The equilibrium oxygen pressure for each system condition is calculated according to the laws of chemical equilibrium as is shown in [61]. The Fe – Si – O state diagram is plotted in two variants. The first one takes into no account the formation of "Fe_3Si" compound and α-phase ordering (as discussed earlier in the section 2. 3.). It is shown **in Fig.2.**

The second variant of the diagram takes into account formation of "Fe_3Si" compound. It is shown **in Fig.3.** The appropriate characteristics of system conditions for the both diagram variants are represented **in table 5.**

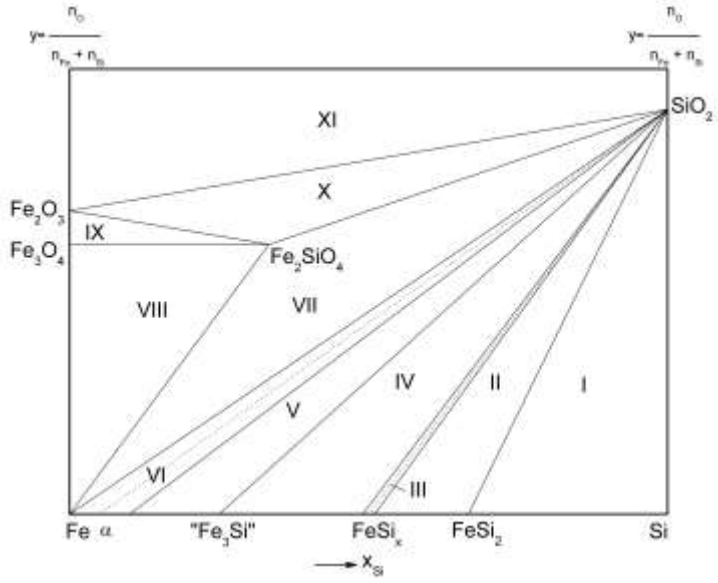

Figure 3. The Fe – Si – O state diagram at 298 K with consideration of "Fe_3Si" drawn up according to the reference data.

Table 5. The characteristics of the Fe – Si – O system conditions at 298 K.

No. of domain at		System condition	Reaction equation	P_{O_2}, bar
figure 2	figure 3			
I	I	$FeSi_2$ – Si (diamond) – SiO_2	Si (diamond) + O_2 = SiO_2	$7.7\cdot10^{-142}$
II	II	$FeSi_{1,033}$ – $FeSi_2$ – SiO_2	$FeSi_2$ + 0,967 O_2 = = $FeSi_{1,033}$ + 0,967 SiO_2	$4.5\cdot10^{-141}$
III	III	$FeSi_x$ – SiO_2 $(0{,}961 \le x \le 1{,}033)$	$FeSi_n$ + $(n-m)$ O_2 = = $FeSi_m$ + $(n-m)$ SiO_2 $(0{,}961 \le m,\ n \le 1{,}033,\ m < n)$	–
IV	–	α-phase (Fe) – $FeSi_{0,961}$ – SiO_2	$FeSi_{0,961}$ + 0,961 O_2 = = Fe (α) + 0,961 SiO_2 $x_{Si(\alpha)} = 0{,}264$; $a_{Si} = 7{,}2\cdot10^{-20}$; $a_{Fe} = 0{,}114$	$1.1\cdot10^{-129}$
–	IV	"Fe_3Si" – $FeSi_{0,961}$ – SiO_2	3$FeSi_{0,961}$ + 1,883 O_2 = = "Fe_3Si" + 1,883 SiO_2	$1.1\cdot10^{-130}$
–	V	α-phase (Fe) – "Fe_3Si" – SiO_2	"Fe3Si" + O_2 = 3Fe (α) + SiO_2 $x_{Si(\alpha)} = 0{,}112$; $a_{Si} = 5{,}5\cdot10^{-20}$; $a_{Fe} = 0{,}473$	$6.4\cdot10^{-126}$
V	VI	α-phase (Fe) – SiO_2	Si (α) + O_2 = SiO_2	–
VI	VII	α-phase (Fe) – Fe_2SiO_4 – SiO_2	2Fe (α) + Si (α) + 2O_2 = Fe_2SiO_4 Si (α) + O_2 = SiO_2 $x_{Si(\alpha)} = 1{,}1\cdot10^{-27}$; $a_{Si} = 5{,}3\cdot10^{-50}$; $a_{Fe} \approx 1$	$1.3\cdot10^{-99}$
VII	VIII	α-phase (Fe) – Fe_3O_4 – [Fe_3O_4, Fe_2SiO_4]	3Fe (α) + 2O_2 = Fe_3O_4 (magnetite) 2Fe (α) + Si (α) + 2O_2 = Fe_2SiO_4	$1.3\cdot10^{-89}$

			Fe_3O_4 (magnetite) = $= Fe_3O_4$ [in Fe_2SiO_4] $x_{Si(\alpha)} = 1{,}02 \cdot 10^{-47}$; $a_{Si} = 4{,}9 \cdot 10^{-70}$; $a_{Fe} \approx 1$; $x_{Fe_3O_4[\text{in } Fe_2SiO_4]} = 6{,}85 \cdot 10^{-5}$; $a_{Fe_3O_4} = 0{,}00233$; $a_{Fe_2SiO_4} \approx 1$	
VIII	IX	$Fe_3O_4 – Fe_2O_3 – [Fe_3O_4, Fe_2SiO_4]$	Fe_3O_4 [in Fe_2SiO_4] = Fe_3O_4 (magnetite) $4Fe_3O_4$ (magnetite) + O_2 = $= 6\ Fe_2O_3$	$2.8 \cdot 10^{-68}$
IX	X	$[SiO_2, Fe_2O_3] – Fe_2SiO_4 – SiO_2$	$2Fe_2SiO_4 + O_2 = 2Fe_2O_3 + 2SiO_2$ (quartz) SiO_2 (quartz) = SiO_2 [in Fe_2O_3] $x_{SiO_2[\text{in } Fe_2O_3]} = 1{,}54 \cdot 10^{-3}$; $a_{Fe_3O_4} = 0{,}0541$; $a_{Fe_2O_3} = 0{,}998$	$1.8 \cdot 10^{-62}$
X	XI	"FeO_2" – SiO_2 – {O_2}	–	–

At domain III, reaction between $FeSi_{1,033}$ phase and oxygen takes place with selective oxidation of silicon. As the result, some silicon oxidizes to SiO_2 and *x* index in $FeSi_x$ formula decreases, until $FeSi_{0,961}$ composition is reached. The similar situation occurs at domain V in Fig. 2 and domain VI in Fig.3, where α-phase reacts with oxygen. Silicon from solid solution oxidizes to SiO_2 and the new solution composition, more and more rich of iron, forms. Both these system conditions are monovariant, therefore equilibrium oxygen pressure changes during reaction and there is no exact value presented in table 5 for these equilibria.

At domain VII in Fig. 2 and domain VIII in Fig. 3 both components of α-phase are oxidized, and simultaneous formation of Fe_3O_4 and Fe_2SiO_4 takes place. A very small amount of magnetite dissolves in fayalite until the maximum solid solubility is reached. The remaining magnetite forms an independent phase. At the next stage (domains VIII and IX in Fig. 2 and 3, respectively) magnetite phase oxidizes to hematite. This causes the equilibrium (35) to shift in the opposite direction; Fe_3O_4 from solid solution transforms back to magnetite and then oxidizes. A similar situation occurs with the second solid solution. At domain IX in Fig. 2 and domain X in Fig. 3 the simultaneous formation of Fe_2O_3 and SiO_2 from Fe_2SiO_4 takes place. A small amount of silicon dioxide dissolves in hematite and the remaining SiO_2 forms a separate phase.

4. Chemical and electrochemical equilibria in Fe – Si – H_2O system under standard conditions and the electrochemical stability of iron silicides

In order to develop thermodynamic model of Fe – Si alloys oxidation in liquid environments, it is convenient to use the diagrams of electrochemical equilibrium (potential – pH dependencies) [61, 81, 82], that most clearly show the possible chemical and electrochemical equilibria in system. Method of plotting such diagrams was described in detail several times [81, 82] and the application of potential – pH diagrams to multicomponent and multiphase equilibria was proposed by the author of [83[. Along the above mentioned oxides, the possible ions that can be formed in the solution, have to be considered as the oxidation products. These ions are Fe^{2+}, Fe^{3+}, FeO_4^{2-} and SiO_3^{2-}.

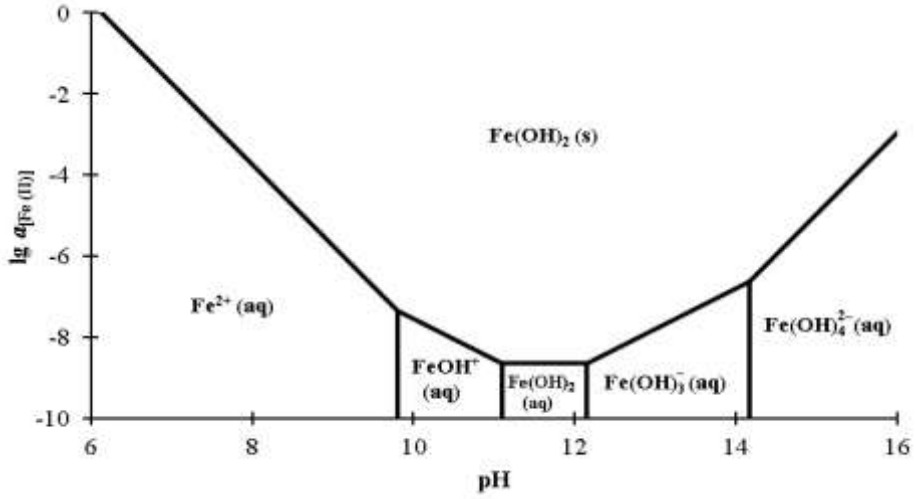

Figure 4. The "activity – pH" diagram for Fe (II) species drawn up according to the reference data.

The $HFeO_2^-$ ion mentioned in the paper [84], can be formed only in strongly alkaline environments (pH > 14) and very dilute solutions ($a_i < 10^{-6}$ mol/l), therefore they are taken into no consideration in the present study. The primary information about the Fe – H_2O and Si – H_2O potential – pH diagrams and the thermodynamic properties of the ion-involving electrochemical reactions can be obtained from textbooks [64, 85], papers [86 – 88] and databases [89 – 97]. The potential – pH diagram for Fe – Si – H_2O system was previously plotted in studies [33, 98], but both of these diagrams take into no account all phases in Fe – Si system.

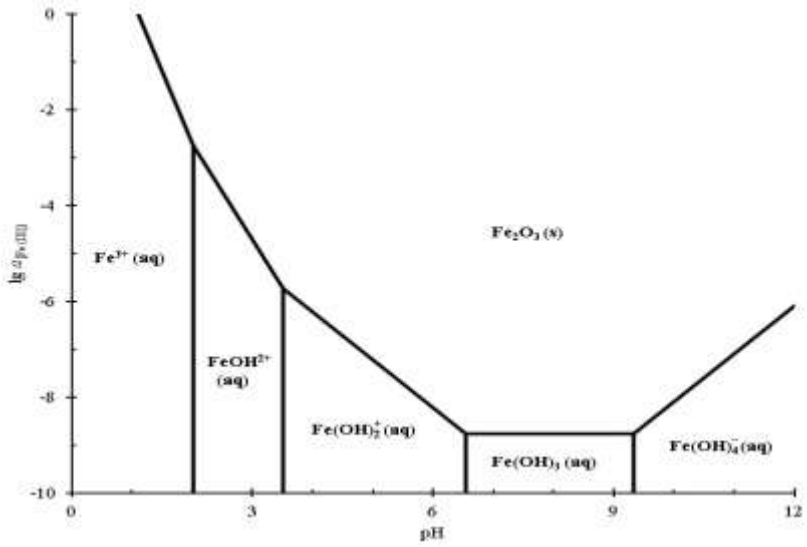

Figure 5. The "activity – pH" diagram for Fe (III) species drawn up according to the reference data.

Any oxides or oxygen-containing ions in the solution can exist in an unhydrated or hydrated form. The transition from the first form to the second one proceeds through the series of intermediate conditions. The thermodynamic stability of various hydrolysis products of ferric and ferrous cations depends on their thermodynamic activities in the solution. The "activity – pH" diagrams for the Fe^{+2} and Fe^{+3} species are presented **in figures 4 and 5**, respectively.

As can be seen from these diagrams, the hydrolyzed forms of ferrous and ferric species are thermodynamically stable only in much diluted solutions at low activity values. Therefore, in the present study the metal hydroxides and the other particles like $FeOH^+$, $FeOOH$, $FeOH^{2+}$, $Fe(OH)_2^+$, $Fe(OH)_3^-$, $Fe(OH)_4^-$, $Fe_2(OH)_2^{4+}$, $Fe_3(OH)_4^{5+}$, H_4SiO_4, H_8SiO_6, $H_2Si_2O_5$, $H_6Si_2O_7$, $HSi(OH)_6^-$, $H_2SiO_4^{2-}$, $H_3SiO_4^-$, $H_4(H_2SiO_4)_4^{4-}$, $H_6(H_2SiO_4)_4^{2-}$, $SiO_2(OH)^{2-}$, $SiO(OH)_3^-$, $Si_2O_3(OH)_4^{2-}$ and others mentioned in [51, 64, 85 – 98], are taken into no consideration, because they are not thermodynamically stable when their activities are equal to 1 $^{mol}/_{l}$.

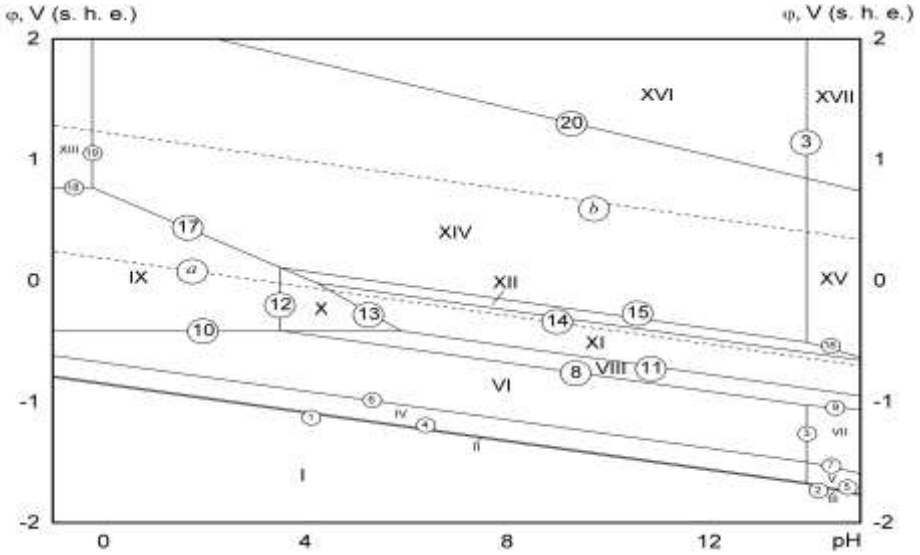

Figure 6. The potential – pH diagram of the Fe – Si – H_2O system at 298 K, air pressure of 1 bar and activities of ions in solutions, equal to 1 $^{mol}/_{l}$ (unhydrated form of oxides, without consideration of "Fe_3Si" compound) drawn up according to the reference data.

The potential – pH diagram of Fe – Si – H_2O system at 25˚C, air pressure of 1 bar and activities of ions in solutions (standard reference state – hypothetical one molar solution), equal to 1 $^{mol}/_{l}$ without consideration of "Fe_3Si" is **shown in Fig. 6**. The characteristics of basic chemical and electrochemical equilibria in system are summarized **in Table 6.**

Table 6. Basic chemical and electrochemical equilibriums in the Fe – Si – H_2O system at 298 K and air pressure of 1 bar, without consideration of "Fe_3Si" compound.

No. of line in Fig. 6	Electrode reaction	Equilibrium potential, V (s. h. e.) or solution pH
a	$2H^+ + 2e^- = H_2; P_{H_2} = 5\cdot10^{-7}\,\text{bar}$	$0.186 - 0.0591\cdot pH$
b	$O_2 + 4H^+ + 4e^- = 2H_2O; P_{O_2} = 0{,}21\,\text{bar}$	$1.219 - 0.0591\cdot pH$
1	$SiO_2 + 4H^+ + 4e^- = Si\ (\text{diamond}) + 2H_2O$	$-0.857 - 0.0591\cdot pH$
2	$SiO_3^{2-} + 6H^+ + 4e^- = Si(\text{diamond}) + 3H_2O$	$-0.444 - 0.0887\cdot pH + 0.0148\cdot \lg a_{SiO_3^{2-}}$
3	$SiO_3^{2-} + 2H^+ = SiO_2 + 2H_2O$	$pH = 13{,}94 + 0{,}5\cdot \lg a_{SiO_3^{2-}}$

4	$FeSi_{1,033} + 0{,}967\ SiO_2 + 3{,}868\ H^+ + 3{,}868\ e^- = FeSi_2 + 1{,}934\ H_2O$	$-0.845 - 0.0591 \cdot pH$
5	$FeSi_{1,033} + 0{,}967\ SiO_3^{2-} + 5{,}802\ H^+ + 3{,}868\ e^- = FeSi_2 + 2{,}901\ H_2O$	$-0.433 - 0.0887 \cdot pH + 0.0148 \cdot \lg a_{SiO_3^{2-}}$
6	$Fe\ (\alpha) + 0{,}961\ SiO_2 + 3{,}844\ H^+ + 3{,}844\ e^- = FeSi_{0,961} + 1{,}922\ H_2O; a_{Fe(\alpha)} = 0{,}114$	$-0.677 - 0.0591 \cdot pH$
7	$Fe\ (\alpha) + 0{,}961\ SiO_3^{2-} + 5{,}766\ H^+ + 3{,}844\ e^- = FeSi_{0,961} + 2{,}883\ H_2O; a_{Fe(\alpha)} = 0{,}114$	$-0.264 - 0.0887 \cdot pH + 0.0148 \cdot \lg a_{SiO_3^{2-}}$
8	$Fe_2SiO_4 + 4H^+ + 4e^- = 2Fe(\alpha) + SiO_2 + 2H_2O;$ $a_{Fe(\alpha)} = 0{,}114$	$-0.205 - 0.0591 \cdot pH$
9	$Fe_2SiO_4 + 2H^+ + 4e^- = 2Fe(\alpha) + SiO_3^{2-} + H_2O;$ $a_{Fe(\alpha)} = 0{,}114$	$-0.617 - 0.0295 \cdot pH - 0.0148 \cdot \lg a_{SiO_3^{2-}}$
10	$Fe^{2+} + 2e^- = Fe(\alpha); a_{Fe(\alpha)} = 0{,}114$	$-0.412 + 0.0295 \cdot \lg a_{Fe^{2+}}$
11	$Fe_3O_4 + 8H^+ + 8e^- = 3Fe(\alpha) + 4H_2O;$ $a_{Fe(\alpha)} = 0{,}114$	$-0.064 - 0.0591 \cdot pH$
12	$Fe_2SiO_4 + 4H^+ = 2Fe^{2+} + SiO_2 + 2H_2O$	$pH = 3.508 - 0.5 \cdot \lg a_{Fe^{2+}}$
13	$Fe_3O_4 + 8H^+ + 2e^- = 3Fe^{2+} + 4H_2O$	$0.982 - 0{,}.364 \cdot pH - 0.0887 \cdot \lg a_{Fe^{2+}}$
14	$3Fe_2O_3 + 2H^+ + 2e^- = 2Fe_3O_4 + H_2O$	$0.231 - 0.0591 \cdot pH$
15	$Fe_2O_3 + SiO_2 + 2H^+ + 2e^- = Fe_2SiO_4 + H_2O$	$0.317 - 0.0591 \cdot pH$
16	$Fe_2O_3 + SiO_3^{2-} + 4H^+ + 2e^- = Fe_2SiO_4 + 2H_2O$	$1.141 - 0.1182 \cdot pH + 0.0295 \cdot \lg a_{SiO_3^{2-}}$
17	$Fe_2O_3 + 6H^+ + 2e^- = 2Fe^{2+} + 3H_2O$	$0.732 - 0.1773 \cdot pH - 0.0591 \cdot \lg a_{Fe^{2+}}$
18	$Fe^{3+} + e^- = Fe^{2+}$	$0.771 + 0.0591 \cdot \lg \frac{a_{Fe^{3+}}}{a_{Fe^{2+}}}$
19	$Fe_2O_3 + 6H^+ = 2Fe^{3+} + 3H_2O$	$pH = -0.221 - 0.333 \cdot \lg a_{Fe^{3+}}$
20	$2FeO_4^{2-} + 10H^+ + 6e^- = Fe_2O_3 + 5H_2O$	$2{,}220 - 0{,}0985 \cdot pH + 0{,}0197 \cdot \lg a_{FeO_4^{2-}}$

17 domains of thermodynamic stability of certain phases are indicated in Diagram (Fig.6):

I – α-phase (bcc) + $FeSi_x$ + $FeSi_2$ + Si (diamond);
II – α-phase (bcc) + $FeSi_x$ + $FeSi_2$ + SiO_2;
III – α-phase (bcc) + $FeSi_x$ + $FeSi_2$ + SiO_3^{2-};
IV – α-phase (bcc) + $FeSi_x$ + SiO_2;
V – α-phase (bcc) + $FeSi_x$ + SiO_3^{2-};

VI – α-phase (bcc) + SiO_2;
VII – α-phase (bcc) + SiO_3^{2-};
VIII – α-phase (bcc) + Fe_2SiO_4;
IX – Fe^{2+} + SiO_2;

X – Fe^{2+} + Fe_2SiO_4;
XI – Fe_3O_4 (magnetite) + [Fe_3O_4, Fe_2SiO_4] (fayalite);
XII – Fe_2O_3 + Fe_2SiO_4;
XIII – Fe^{3+} + SiO_2;
XIV – [SiO_2, Fe_2O_3] (hematite) + SiO_2 (quartz);
XV – Fe_2O_3 + SiO_3^{2-};
XVI – FeO_4^{2-} + SiO_2;
XVII – FeO_4^{2-}, SiO_3^{2-}.

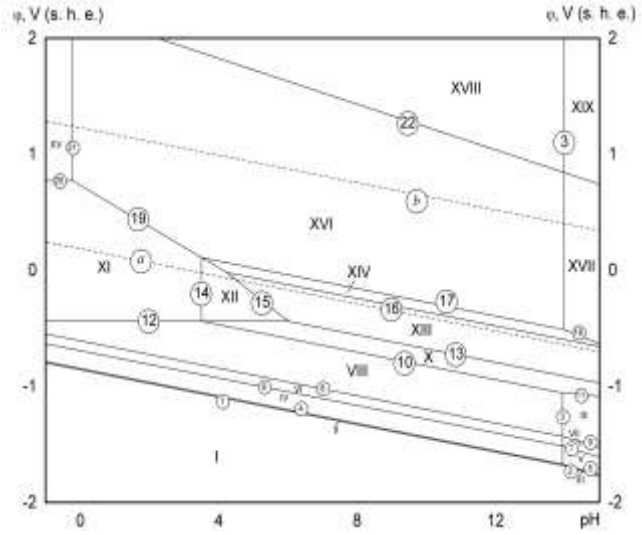

Figure 7. The potential – pH diagram of the Fe – Si – H_2O system at 298 K, air pressure of 1 bar and activities of ions in solutions, equal to 1 $^{mol}/_{l}$ (unhydrated form of oxides subject to "Fe_3Si" compound), designed according to the reference data.

Domain I is the one of thermodynamic stability where all components of Fe – Si system remain immune to corrosion. At the domains from II to VII the consecutive decomposition of iron silicides takes place. Domains IX, X and XIII are the ones of active corrosion, where iron dissolves from alloys and passes into solution in the form of cations Fe^{2+} or Fe^{3+}. Domains II, IV, VI, VIII, XI, XII, XIV and XVI are the ones of passivity where the protective oxide film, consisting of simple oxides of iron or silicon or iron silicate, is formed on the alloy surface to prevent further oxidation. Domains III, V, VII, XV and XVII are the ones of transpassivity, where the oxides from passivation layer oxidize further and pass into solution in the form of anions which violates the integrity of the protective film.

The potential – pH diagram of Fe – Si – H_2O system at 25°C, air pressure of 1 bar and activities of ions in the solutions equal to 1 $^{mol}/_{l}$, considering "Fe_3Si", is presented **in Fig. 7.** The characteristics of appropriate chemical and electrochemical equilibria in the system are summarized **in Table 7.**

Table 7. Basic chemical and electrochemical equilibria in the Fe – Si – H_2O system at 298 K and air pressure of 1 bar allowing for "Fe_3Si" compound

No. of line in Fig. 7	Electrode reaction	Equilibrium potential, V (s. h. e.) or solution pH
a	$2H^+ + 2e^- = H_2; P_{H_2} = 5\cdot10^{-7}$ bar	$0{,}186 - 0{,}0591\cdot pH$
b	$O_2 + 4H^+ + 4e^- = 2H_2O; P_{O_2} = 0{,}21$bar	$1{,}219 - 0{,}0591\cdot pH$
1	$SiO_2 + 4H^+ + 4e^- = Si\ (diamond) + 2H_2O$	$-0{,}857 - 0{,}0591\cdot pH$
2	$SiO_3^{2-} + 6H^+ + 4e^- = Si(diamond) + 3H_2O$	$-0{,}444 - 0{,}0887\cdot pH + 0{,}0148\cdot \lg a_{SiO_3^{2-}}$

3	$SiO_3^{2-} + 2H^+ = SiO_2 + 2H_2O$	$pH = 13{,}94 + 0{,}5 \cdot \lg a_{SiO_3^{2-}}$
4	$FeSi_{1,033} + 0{,}967\ SiO_2 + 3{,}868\ H^+ + 3{,}868\ e^- =$ $= FeSi_2 + 1{,}934\ H_2O$	$-0{,}845 - 0{,}0591 \cdot pH$
5	$FeSi_{1,033} + 0{,}967\ SiO_3^{2-} + 5{,}802\ H^+ + 3{,}868\ e^- =$ $= FeSi_2 + 2{,}901\ H_2O$	$-0{,}433 - 0{,}0887 \cdot pH + 0{,}0148 \cdot \lg a_{SiO_3^{2-}}$
6	$"Fe_3Si" + 1{,}883\ SiO_2 + 7{,}532\ H^+ + 7{,}532\ e^- =$ $= 3FeSi_{0,961} + 3{,}766\ H_2O$	$-0{,}692 - 0{,}0591 \cdot pH$
7	$"Fe_3Si" + 1{,}883\ SiO_3^{2-} + 11{,}298\ H^+ + 7{,}532\ e^- =$ $= FeSi_{0,961} + 5{,}649\ H_2O$	$-0{,}279 - 0{,}0887 \cdot pH + 0{,}0148 \cdot \lg a_{SiO_3^{2-}}$
8	$3Fe\ (\alpha) + SiO_2 + 4H^+ + 4e^- =$ $= "Fe_3Si" + 2H_2O; a_{Fe(\alpha)} = 0{,}456$	$-0{,}622 - 0{,}0591 \cdot pH$
9	$3Fe\ (\alpha) + SiO_3^{2-} + 6H^+ + 4e^- =$ $= "Fe_3Si" + 3H_2O; a_{Fe(\alpha)} = 0{,}456$	$-0{,}210 - 0{,}0887 \cdot pH + 0{,}0148 \cdot \lg a_{SiO_3^{2-}}$
10	$Fe_2SiO_4 + 4H^+ + 4e^- = 2Fe(\alpha) + SiO_2 + 2H_2O;$ $a_{Fe(\alpha)} = 0{,}456$	$-0{,}222 - 0{,}0591 \cdot pH$
11	$Fe_2SiO_4 + 2H^+ + 4e^- = 2Fe(\alpha) + SiO_3^{2-} + H_2O;$ $a_{Fe(\alpha)} = 0{,}456$	$-0{,}635 - 0{,}0295 \cdot pH - 0{,}0148 \cdot \lg a_{SiO_3^{2-}}$
12	$Fe^{2+} + 2e^- = Fe(\alpha); a_{Fe(\alpha)} = 0{,}456$	$-0{,}430 + 0{,}0295 \cdot \lg a_{Fe^{2+}}$
13	$Fe_3O_4 + 8H^+ + 8e^- = 3Fe(\alpha) + 4H_2O;$ $a_{Fe(\alpha)} = 0{,}456$	$-0{,}077 - 0{,}0591 \cdot pH$
14	$Fe_2SiO_4 + 4H^+ = 2Fe^{2+} + SiO_2 + 2H_2O$	$pH = 3{,}508 - 0{,}5 \cdot \lg a_{Fe^{2+}}$
15	$Fe_3O_4 + 8H^+ + 2e^- = 3Fe^{2+} + 4H_2O$	$0{,}982 - 0{,}2364 \cdot pH - 0{,}0887 \cdot \lg a_{Fe^{2+}}$
16	$3Fe_2O_3 + 2H^+ + 2e^- = 2Fe_3O_4 + H_2O$	$0{,}231 - 0{,}0591 \cdot pH$
17	$Fe_2O_3 + SiO_2 + 2H^+ + 2e^- = Fe_2SiO_4 + H_2O$	$0{,}317 - 0{,}0591 \cdot pH$
18	$Fe_2O_3 + SiO_3^{2-} + 4H^+ + 2e^- = Fe_2SiO_4 + 2H_2O$	$1{,}141 - 0{,}1182 \cdot pH + 0{,}0295 \cdot \lg a_{SiO_3^{2-}}$
19	$Fe_2O_3 + 6H^+ + 2e^- = 2Fe^{2+} + 3H_2O$	$0{,}732 - 0{,}1773 \cdot pH - 0{,}0591 \cdot \lg a_{Fe^{2+}}$
20	$Fe^{3+} + e^- = Fe^{2+}$	$0{,}771 + 0{,}0591 \cdot \lg \frac{a_{Fe^{3+}}}{a_{Fe^{2+}}}$
21	$Fe_2O_3 + 6H^+ = 2Fe^{3+} + 3H_2O$	$pH = -0{,}221 - 0{,}333 \cdot \lg a_{Fe^{3+}}$
22	$2FeO_4^{2-} + 10H^+ + 6e^- = Fe_2O_3 + 5H_2O$	$2{,}220 - 0{,}0985 \cdot pH + 0{,}0197 \cdot \lg a_{FeO_4^{2-}}$

Diagram in Fig. 7 contains 19 domains of thermodynamic stability in certain phases:

I – α-phase (bcc) + "Fe_3Si" + $FeSi_x$ + $FeSi_2$ + Si (diamond);
II – α-phase (bcc) + "Fe_3Si" + $FeSi_x$ + $FeSi_2$ + SiO_2;
III – α-phase (bcc) + "Fe_3Si" + $FeSi_x$ + $FeSi_2$ + SiO_3^{2-};
IV – α-phase (bcc) + "Fe_3Si" + $FeSi_x$ + SiO_2;
V – α-phase (bcc) + "Fe_3Si" + $FeSi_x$ + SiO_3^{2-};
VI – α-phase (bcc) + "Fe_3Si" + SiO_2;
VII – α-phase (bcc) + "Fe_3Si" + SiO_3^{2-};
VIII – α-phase (bcc) + SiO_2;
IX – α-phase (bcc) + SiO_3^{2-};
X – α-phase (bcc) + Fe_2SiO_4;
XI – Fe^{2+} + SiO_2;
XII – Fe^{2+} + Fe_2SiO_4;
XIII – Fe_3O_4 (magnetite) + [Fe_3O_4, Fe_2SiO_4] (fayalite);
XIV – Fe_2O_3 + Fe_2SiO_4;
XV – Fe^{3+} + SiO_2;
XVI – [SiO_2, Fe_2O_3] (hematite) + SiO_2 (quartz);
XVII – Fe_2O_3 + SiO_3^{2-};
XVIII – FeO_4^{2-} + SiO_2;
XIX – FeO_4^{2-}, SiO_3^{2-}.

There are minor differences between Diagrams in Fig. 6 and 7 related to the "Fe_3Si" phase. The equilibriums in Fig. involving α-Fe (lines 8 through 11 in Fig. 6 and lines 10 through 13 in Fig. 7) differ by 0,02V due to different activities of iron in solid solutions. The equilibriums involving oxide phases (lines 12 – 20 and 14 – 22, respectively) are quite the same. Consequently, the classification of domains in Fig. 7 is identical to the one shown in Fig. 6. In addition to domains I through V in Fig. 6 there are two extra domains, exactly VI and VII in Fig. 7 that correspond to "Fe_3Si" compound stability. Domains VI through XVII in Fig. 6 and domains VIII through XIX in Fig. 7 are identical with the same areas of active corrosion, passivity and trans-passivity.

Along with electrochemical oxidation into oxides or anions, the electrochemical reduction of metal compounds into their hydrides can occur in water environment. Therefore, possible formation of iron and silicon hydrides is taken into consideration. It is well known that iron hydride exists within the Earth's core at high pressures and temperatures [99, 100]. But its synthesis at standard temperature was also studied by the authors of [100, 101]. Iron hydride has hcp structure and the variable composition FeH_x $\{0 < x \le 1\}$ [100, 101]. Index "x" strongly depends on the sample synthesis conditions, for example, $FeH_{0,3}$ – $FeH_{0,4}$ was reported in [100] and the variety ranging from $FeH_{0,1}$ to $FeH_{0,8}$ in [101]. There are a few studies of iron hydride thermodynamic properties [102, 103] since its standard Gibbs energy of formation cannot be determined directly. The authors of [102] performed an estimation of the value with reference to stoichiometric compound "FeH". The result of their estimation is as follows:

$$\Delta_f G^o_{298}(\text{"FeH"}) = 23500 \text{ J mol}^{-1} \quad (52).$$

Silicon hydrides SiH_2, SiH_4 and Si_2H_6 can be produced only at 120ºC, they resist any chemical influence of water environments (unless there are no fluoride ions in solution) and can't be formed electrochemically [65]. Therefore, only equilibria, involving iron hydride are considered in present study.

Calculations show, that "Fe_3Si" compound isn't thermodynamically stable in presence of iron hydride. Therefore, it isn't taken into consideration, and the first variant of Fe – Si system potential – pH diagram, presented in Fig. 6, is modified in order to consider possible electrochemical formation of iron hydride. The potential – pH diagram of Fe – Si – H_2O system at 25˚C, air pressure of 1 bar and activities of ions in the solutions equal to 1 mol l^{-1}, with due regard for "FeH", is presented in Fig. 8. The characteristics of appropriate chemical and electrochemical equilibria in system are summarized **in Table 8.**

Table 8. Basic chemical and electrochemical equilibriums in the Fe – Si – H_2O system at 298 K and air pressure of 1 bar with due regard for "FeH" compound.

No. of line in Fig. 8	Electrode reaction	Equilibrium potential, V (s. h. e.) or solution pH
a	$2H^+ + 2e^- = H_2; P_{H_2} = 5\cdot10^{-7}$ bar	$0.186 - 0.0591\cdot pH$
b	$O_2 + 4H^+ + 4e^- = 2H_2O; P_{O_2} = 0{,}21$ bar	$1.219 - 0.0591\cdot pH$
1	$FeSi_2 + H^+ + e^- = "FeH" + 2Si$ (diamond)	$-1.064 - 0.0591\cdot pH$
2	$2\ FeSi_{1,033} + 0{,}967\ H^+ + 0{,}967\ e^- = 0{,}967\ "FeH" + 1{,}033\ FeSi_2$	$-0.974 - 0.0591\cdot pH$
3	$0{,}961\ Fe_2SiO_4 + 8{,}61\ H^+ + 8{,}61\ e^- = FeSi_{0,961} + 0{,}922\ "FeH" + 3{,}844\ H_2O$	$-0.426 - 0.0591\cdot pH$
4	$Fe^{2+} + H^+ + 3e^- = "FeH"$	$-0.375 - 0.0197\cdot pH + 0.0197\cdot \lg a_{Fe^{2+}}$
5	$Fe(\alpha) + H^+ + e^- = "FeH"; a_{Fe(\alpha)} = 0{,}114$	$-0.299 - 0.0591\cdot pH$
6	$Fe^{2+} + 2e^- = Fe(\alpha); a_{Fe(\alpha)} = 0{,}114$	$-0.412 + 0.0295\cdot \lg a_{Fe^{2+}}$
7	$Fe_3O_4 + 8H^+ + 8e^- = 3Fe(\alpha) + 4H_2O;$ $a_{Fe(\alpha)} = 0{,}114$	$-0.064 - 0.0591\cdot pH$
8	$Fe_2SiO_4 + 4H^+ = 2Fe^{2+} + SiO_2 + 2H_2O$	$pH = 3.508 - 0.5\cdot \lg a_{Fe^{2+}}$
9	$Fe_3O_4 + 8H^+ + 2e^- = 3Fe^{2+} + 4H_2O$	$0.982 - 0.2364\cdot pH - 0.0887\cdot \lg a_{Fe^{2+}}$
10	$3Fe_2O_3 + 2H^+ + 2e^- = 2Fe_3O_4 + H_2O$	$0.231 - 0.0591\cdot pH$
11	$Fe_2O_3 + SiO_2 + 2H^+ + 2e^- = Fe_2SiO_4 + H_2O$	$0.317 - 0.0591\cdot pH$
12	$Fe_2O_3 + SiO_3^{2-} + 4H^+ + 2e^- = Fe_2SiO_4 + 2H_2O$	$1.141 - 0.1182\cdot pH + 0.0295\cdot \lg a_{SiO_3^{2-}}$
13	$SiO_3^{2-} + 2H^+ = SiO_2 + 2H_2O$	$pH = 13.94 + 0.5\cdot \lg a_{SiO_3^{2-}}$
14	$Fe_2O_3 + 6H^+ + 2e^- = 2Fe^{2+} + 3H_2O$	$0.732 - 0.1773\cdot pH - 0.0591\cdot \lg a_{Fe^{2+}}$
15	$Fe^{3+} + e^- = Fe^{2+}$	$0.771 + 0.0591\cdot \lg \frac{a_{Fe^{3+}}}{a_{Fe^{2+}}}$
16	$Fe_2O_3 + 6H^+ = 2Fe^{3+} + 3H_2O$	$pH = -0.221 - 0.333\cdot \lg a_{Fe^{3+}}$
17	$2FeO_4^{2-} + 10H^+ + 6e^- = Fe_2O_3 + 5H_2O$	$2{,}220 - 0{,}0985\cdot pH + 0{,}0197\cdot \lg a_{FeO_4^{2-}}$

The presence of "FeH" changes and simplifies the scheme of iron silicides decomposition; there are only 14 domains of thermodynamic stability of certain phases:

I – "FeH" + $FeSi_x$ + $FeSi_2$ + Si (diamond);
II – "FeH" + $FeSi_x$ + $FeSi_2$;
III – "FeH" + $FeSi_x$;
IV – "FeH" + Fe_2SiO_4;
V – α-phase (bcc) + Fe_2SiO_4;
VI – Fe^{2+} + SiO_2;
VII – Fe^{2+} + Fe_2SiO_4;
VIII – Fe_3O_4 (magnetite) + [Fe_3O_4, Fe_2SiO_4] (fayalite);
IX – Fe_2O_3 + Fe_2SiO_4;
X – Fe^{3+} + SiO_2;
XI – [SiO_2, Fe_2O_3] (hematite) + SiO_2 (quartz);
XII – Fe_2O_3 + SiO_3^{2-};
XIII – FeO_4^{2-} + SiO_2;

XIV – FeO_4^{2-}, SiO_3^{2-}.

According to the calculations, silicon dioxide and iron hydride cannot coexist. Another scheme of iron silicides oxidation is presented (lines 1 – 5 at the diagram), without formation of SiO_2 and SiO_3^{2-}. Instead of domains I through VII in Fig. 6 only another domains I through IV are depicted in Fig. 8. These domains can be also classified as domains of passivity of Fe – Si alloy components where the passivation film consists of iron hydride as opposed to any oxides. The consideration of "FeH" does not affect all equilibriums which take place in Fe – Si – H_2O system after Fe_2SiO_4 was formed. The lines 6 through 17 and the domains V through XIV in Fig. 8 are identical to the lines 10 through 20 and the domains VIII through XVII in Fig. 6.

5. Results and discussion

The partial pressure of oxygen in atmospheric air is equal to 0,21 bar under standard conditions. This means that all equilibria in Fe – Si – O system over which equilibrium oxygen pressure is less than 0,21 bar, take place in air environments. Table 5 shows that oxidation of Fe – Si system alloys ends with the formation of Fe_2O_3 and SiO_2 (domains IX and X in Fig. 2 and 3 respectively) and this agrees with information given in [65]. A smaller part of SiO_2 can be dissolved in Fe_2O_3 while another part forms an independent quartz phase.

The specific composition of oxide layer on Fe – Si alloys depends on their composition. Silicon oxidizes in the first order but if its content in alloy is insufficient to form a continuous passivation layer, Fe_2O_3 can also be involved in its formation. Even Fe_2SiO_4 can be presented in protective film in the form of local inclusions due to the kinetic factors and unreachability of the true equilibrium.

The oxidation features of iron-silicon alloys with variable silicon contents therein were studied experimentally several times [104 – 112]; however, these studies deal with high temperatures (800 – 1100ºC). It was revealed [109, 111, 112] that due to a very low diffusibility of iron through a silica film, the oxidation rate of Fe – Si alloys is much lower than that of pure iron and typical Cr_2O_3-forming alloy Fe-26Cr. Oxidation rates become increasingly slower as the silicon content in alloy exceeds ~5 weight percent [111]. It is related to the minimum silicon concentration sufficient to develop and maintain a continuous SiO_2 layer on alloy surface [110]. Theoretical studies [32] predict that this minimum concentration is precisely 5 weight percent at temperatures of 400 – 1000 K. For the alloys composition with lesser silicon content [105 – 108, 112], the presence of Fe_2O_3, Fe_3O_4 and Fe_2SiO_4 is also detected in oxide layer. The primary passivation film made of SiO_2, can, however, decompose, if a significant amount of CO_2 is presented in atmosphere [106 – 110].

When analyzing Fe – Si alloys electrochemical oxidation, it is important to single out lines *a* and *b* in potential – pH Diagrams. They correspond to hydrogen and oxygen electrodes, respectively. An area between these two lines corresponds to water electrochemical stability and matters most in exploring the corrosion processes. In Diagrams presented in Fig. 6 – 8, an area of water electrochemical stability is the same with/without regard to some compounds. In strongly acidic environments (pH < 3) iron oxidizes to Fe^{2+} or Fe^{3+} cations, and only in very alkaline environments (pH > 14) silicate ions can be produced. A greater part of this area is occupied by the domain of thermodynamic stability of Fe_2O_3 + SiO_2 which corresponds to rather large passivity region. The author of [33] declares that there are three stages of the oxidation process involving SiO_2, Fe_2SiO_4 and iron oxides. This is a doubtful suggestion, because, in contrast to some other transition metals silicates [113 – 117], iron silicate has a very narrow field of thermodynamic stability and plays a minor role in Fe – Si alloys corrosion-electrochemical behavior in the area of water stability. Moreover, Fe_2SiO_4 is treated as metastable compound in water environments

and excluded from considerations in the study [98]. Conclusions made earlier for chemical stability of iron silicides in regard of Fe_2O_3 and SiO_2-containing passivation film are valid for electrochemical corrosion as well.

However, some aspects of electrochemical behavior of Fe – Si system outside the area of water stability are not so clear. The oxidation of Fe^{+3} to Fe^{+6} takes place at the very high potentials greater than 2V that are very hard to achieve experimentally. Therefore, there is no experimental evidences that prove or disprove the possible formation of iron (IV) aqueous species as the intermediates between iron (III) and iron (IV) species.

Note that equilibriums involving iron hydride "FeH" have also predictive nature. There is no data in literature on electrochemical formation of hydride that can verify these calculations which are rather approximate because thermodynamic properties of "FeH" are just estimated rather than directly determined. Consecutive schemes of decomposition of iron silicides with/without iron hydride vary from each other essentially, so an exact mechanism of these processes remains open for discussion.

It has to be kept in mind that corrosion properties of Fe – Si systems were studied thoroughly, including corrosion rate measurements and polarization tests on various iron silicides [118 – 129], particularly in acidic [118 – 122] and alkaline [127 – 129] environments, corrosion studies of Fe – Si solid solutions [130], studies of oxidation products [131 – 133] and corrosion properties of multicomponent alloys, coatings, films and other complicated wares, including iron-silicon system [134 – 140]. Thermodynamic calculations performed in the present study are not contrary to experimental data presented in the paper. For all iron silicides where the silicon content is high enough, in acidic electrolytes, iron selectively dissolves from the silicide sub-lattice forming cations while silicon remains on the surface and forms a SiO_2 film notable for high electrochemical resistance (certainly, if there is no fluoride-ions in the solution). Later on, the process is limited by the diffusion of metal atoms from the bulk of the silicide toward the surface layer and the diffusion of oxidized metal through the film of hydrated silicon hydroxide. In alkaline electrolytes, the solubility of silicon and silicon dioxide sharply increases, and the mechanism of the anodic process is determined by the formation of protective films composed of Fe_3O_4 and FeOOH. The films passivate the surface and make the silicides stable against alkalis. The minimal silicon concentration that allows forming protective SiO_2 films in acids for Fe – Si containing alloys, is about 5 weight percent.

Despite the lack of reliable information, thermodynamic theory cannot yet give a clear answer to the all aspects of chemical and electrochemical stability of Fe – Si system alloys, just basic regularities are revealed and analyzed. Thermodynamic description can successfully complement and broaden the results of corrosion experiments.

Conclusions

1. Thermodynamic properties of Fe – Si system at 298 K were analyzed, the comparison between available thermodynamic descriptions was made and the thermodynamic estimation of the Gibbs energy of formation of non-stoichiometric iron silicide explored. Also, the thermodynamic analysis of the long-distance ordering in the system at low temperatures was performed and the maximum solid solubility of silicon in bcc-Fe at 298 K estimated. It equals to 26 atomic percent provided that "Fe_3Si" is taken into no account as independent compound together with 11 atomic percent if it is.

2. The Fe – Si – O state diagram at 298 K was plotted and the invariant system conditions calculated. Besides, the maximum solid solubility of Fe_2SiO_4 in Fe_3O_4 and of SiO_2 in Fe_2O_3 at 298 K was estimated and the activity of – pH diagrams for the ferrous and ferric aqueous species and the potential – pH diagrams of Fe – Si – H_2O system at 298 K, air pressure of 1 bar and activities of ions in solution, equal to 1 $^{mol}/_{l}$ with/without

consideration of "Fe_3Si" and "FeH". The characteristics of the basic chemical and electrochemical equilibrium in Fe – Si – H_2O system were calculated.

3. Thermodynamic analysis of chemical and electrochemical stability of iron – silicon system alloys was performed and positive influence of silicon on iron corrosion properties revealed.

References

1. Shein A.B. Electrochemistry of transition metals silicides and germanides. Perm: Publishing House of Perm State University, 2009. (In Russian).
2. Morales A.M., Lieber C.M. A Laser Ablation Method for the Synthesis of Crystalline Semiconductor Nanowires. *Science*, 1998, vol. 279, pp. 208-211.
3. Milosavljević M., Shao G., Bibić N., McKinty C.N., Jeynes C. et al. Amorphous-iron disilicide: A promising semiconductor. *Applied Physics Letters*. 2001, vol. 79, no. 10, pp. 1438 – 1440.
4. Novet T., Johnson D.C. New Synthetic Approach to Extended Solids: Selective Synthesis of Iron Silicides via the Amorphous State. *Journal of the American Chemical Society*. 1991, vol. 113, no. 9, pp. 3398-3403.
5. Mandrus D., Sarrao J.L., Migliori A., Thompson J.D., Fisk Z. Thermodynamics of FeSi. *Physical Review B*, 1995, vol. 51, no. 8, pp. 4763-4767.
6. Paschen S. et al. Low-temperature transport, thermodynamic and optical properties of FeSi, *Physical Review B*. 1997, vol. 56, no. 20, pp. 12916-12930.
7. Patrin G.S. et al. Nonstoichiometry and Low-Temperature Magnetic Properties of FeSi Crystals. *Physics of the Solid State*. 2006, vol. 48, no. 4, pp. 700-704.
8. Lin J.-F., Heinz D. L., Campbell A. J., Devine J. M., Shen G. Iron-Silicon Alloy in Earth's Core? *Science*. 2002, vol. 295, pp. 313-315.
9. Lau S.S., Feng J.S.-Y., Olowolafe J.O., Nicolet M.-A. Iron Silicide Thin Film Formation at Low Temperatures. *Thin Solid Films*. 1975, vol. 25, pp. 415-422.
10. Hu J., Odom T.W., Lieber C.M. Chemistry and Physics in One Dimension: Synthesis and Properties of Nanowires and Nanotubes. *Accounts of Chemical Research*. 1999, vol. 32, no. 5, pp. 435-445.
11. V. Raghavan. Fe-Ni-Si (Iron-Nickel-Silicon). *Journal of Phase Equilibria*. 2003, vol. 24, no. 3, pp. 269 – 271.
12. Du Y., Schuster J.C. et al. A thermodynamic description of the Al – Fe – Si system over the whole composition and temperature ranges via a hybrid approach of CALPHAD and key experiments. *Intermetallics*. 2008, vol. 16, pp. 554 – 570.
13. Liu Z.-K., Chang Y.A. Thermodynamic Assessment of the Al-Fe-Si System. *Metallurgical and Materials Transactions A*. 1999, vol. 30A, pp. 1081 – 1095.
14. Raghavan V. Al-Fe-Si (Aluminium-Iron-Silicon). *Journal of Phase Equilibria*. 2002, vol. 22, no. 4, pp. 362 – 366.
15. Forsberg A., Ågren J. Thermodynamics, Phase Equilibria and Martensitic Transformation in Fe-Mn-Si Alloys. *Materials Research Society Symposium Proceedings*. 1992, vol. 246, pp. 289 – 295.
16. Forsberg A., Ågren J. Thermodynamic Evaluation of the Fe-Mn-Si System and the γ/ε Martensitic Transformation. *Journal of Phase Equilibria*. 1993, vol. 14, no. 3, pp. 354 – 363.
17. Hino M., Nagasaka T., Washizu T. Phase Diagram of Fe-Cu-Si Ternary System above 1523 K. *Journal of Phase Equilibria*. 1999, vol. 20, no. 3, pp. 179 – 186.
18. Zhao J., Zhang L. et al. Experimental Investigation and Thermodynamic Reassessment of the Cu-Fe-Si System. *Metallurgical and Materials Transactions A*. 2009, vol. 40A, pp. 1811 – 1825.
19. Raghavan V. Cr-Fe-Si (Chromium-Iron-Silicon). *Journal of Phase Equilibria*. 2003, vol. 24, no. 3, pp. 265 – 266.

20. Perrot P., Dauphin J.Y. Calculation of the Fe-Zn-Si Phase Diagram between 773 and 1173 K, *CALPHAD*, 1988, vol. 12, no. 1, pp. 33 – 40.
21. Su X., Tang N.-Y., Toguri M J. 450ºC Isothermal Section Of the Fe-Zn-Si Ternary Phase Diagram. *Canadian Metallurgical Quarterly*. 2001, vol. 40, no. 3, pp. 377 – 384.
22. Su X., Yin F., Li Z., Tang N.-Y., Zhao M.. Thermodynamic calculation of the Fe–Zn–Si system. *Journal of Alloys and Compounds*. 2005, vol. 396, pp. 156 – 163.
23. Lacaze J., Sundman B. An Assessment of the Fe-C-Si System. *Metallurgical and Materials Transactions A*. 1991, vol. 22A, pp. 2211 – 2223.
24. Wada T., Wada H., Elliott J. F., Chipman J. Thermodynamics of the FCC Fe-Mn-C and Fe-Si-C Alloys. *Metallurgical and Materials Transactions*. 1972, vol. 3, pp. 1657 – 1662.
25. Miettinen J. Reassessed Thermodynamic Solution Phase Data for Ternary Fe-Si-C System. *CALPHAD*. 1998, vol. 22, no. 2, pp. 231 – 256.
26. Shaposhnikov N.G., Mogutnov B.M. Paraequilibria in the Fe–Si–C System and Their Relation to the Bainite Transformation in Steels. *Russian Metallurgy (Metally)*. 2008, vol. 2008, no. 2, pp. 174 – 179.
27. Myers J., Eugster H.P. The System Fe-Si-O: Oxygen Buffer Calibrations to 1,500K. *Contribution to Mineralogy and Petrology*. 1983, vol. 82, pp. 75 – 90.
28. Fabrichnaya O.B., Sundman B. The assessmeut of thermodynamic parameters in the Fe-O and Fe-Si-O systems. *Geochimica et Cosmochimica Acta*. 1997, vol. 61, no. 21, pp. 4539 – 4555.
29. Tokunaga T., Ohtani H., Hasebe M. Thermodynamic evaluation of the phase equilibria and glass-forming ability of the Fe–Si–B system. *CALPHAD: Computer Coupling of Phase Diagrams and Thermochemistry*. 2004, vol. 28, pp. 354 – 362.
30. Zaitsev A.I., Zaitseva N.E. Thermodynamic Study of Liquid Fe–Si–B Alloys: The Effect of Ternary Associated Groups on Transformation of the Alloy into the Amorphous State. *Doklady Physical Chemistry*. 2002, vol. 384, no. 4 – 6, pp. 126 – 130.
31. Anglezio J.C., Servant C., Ansara I. Contribution to the Experimental and Thermodynamic Assessment of the Al – Ca – Fe – Si system – I. Al – Ca – Fe, Al – Ca – Si, Al – Fe – Si and Ca – Fe – Si systems. *CALPHAD*. 1994, vol. 18, no. 3, pp. 273 – 309.
32. Atkinson A. A theoretical analysis of the oxidation of Fe – Si alloys. *Corrosion Science*. 1982, vol. 22, no. 2, pp. 87 – 102.
33. Tyurin A.G. Thermodynamic evaluation of silicon influence on chemical and electrochemical stability of iron-chromium alloys. *Protection of Metals*. 2004, vol. 40, no. 1, pp. 14 – 22.
34. Phase Diagrams of Binary Metallic Systems / Editor N. P. Lyakishev. Moscow: Mashinostroenie Publ. 1997, vol. 2. P. 551 – 554. (In Russian)
35. Phase diagram – Web. Fact Sage Database. URL: <http://www.crct.polymtl.ca/fact/documentation>.
36. Gude A., Mehrer H. Diffusion in the $D0_3$-type intermetallic phase Fe_3Si. *Philosophical Magazine A*. 1997, vol. 76, no. 1, pp. 1 – 29.
37. Haggstrom L., Grinas L., Wappling R., Devanarayanan S. Mössbauer Study of Ordering in FeSi Alloys. *Physica Scripta*. 1973, vol. 7, pp. 125 – 131.
38. Lee B.-J., Lee S.K., Lee D.N. Formulation of the A2/B2/$D0_3$ Atomic Ordering Energy and a Thermodynamic Analysis of the Fe-Si System. *CALPHAD*. 1987, vol. 11, no. 2, pp. 253 – 270.
39. Sakao H., Elliott J.F. Thermodynamics of Dilute bcc Fe-Si Alloys. *Metallurgical and Materials Transactions A*. 1975, vol. 6A, pp. 1849 – 1851.
40. Chipman J., Fulton J.C., Gokcen N., Caskey G.R., Jr. Activity of Silicon in Liquid Fe-Si and Fe-C-Si Alloys. *Acta Metallurgica*. 1954, vol. 2, pp. 439 – 450.

41. Fruehan R.J. The Thermodynamic Properties of Liquid Fe-Si Alloys. *Metallurgical Transactions*. 1970, vol. 1, pp. 865 – 870.
42. Hilfrich K. et al. Revision of the Fe-Si phase diagram: No B2-phase for $7.6\ \text{at.\%} \le c_{Si} \le 10.2\ \text{at.\%}$. *Scripta Metallurgica et Materialia*. 1990, vol. 24, no. 1, pp. 39 – 44.
43. Kaufman L. Coupled Phase Diagrams and Thermochemical Data for Transition Metal Binary System – VI. *CALPHAD*. 1979, vol. 3, no. 1, pp. 45 – 76.
44. Sundman B., Ågren J. A regular solution model for phases with several components and sublattices suitable for computer applications. *Journal of Physical Chemistry of Solids*. 1981, vol. 42, pp. 297 – 301.
45. Laptev D.M. Thermodynamics of Metallurgical Solutions Chelyabinsk: Metallurgija Publ. 1992. (In Russian).
46. Redlich O., Kister A.T. Algebraic representation of thermodynamic properties and the classification of solutions, *Industrial and Engineering Chemistry*, 1948, vol. 40, no. 2, pp. 345 – 348.
47. Dinsdale A.T. SGTE Data for Pure Elements. *CALPHAD*. 1991, vol. 15, no. 4, pp. 317 – 425.
48. Zhuk N. P. Textbook on the Theory of Corrosion and Metal Protection. University Course Moscow: Al'yans Publ. 2006. (In Russian).
49. Nikolaychuk P.A., Tyurin A.G. Method of estimating the standard Gibbs energies of formation of binary compounds. *Abstracts of the XVIII International Conference on Chemical Thermodynamics in Russia (RCCT-2011)*. Samara, 2011, vol. 2, pp. 16 – 17.
50. Ruzinov L.P., Gulyanitskii B.S. Equilibrium Transformations in Metallurgical Reactions: Handbook Moscow: Metallurgiya Publ. 1975. (In Russian).
51. Thermal Constants of Substances: Database. – URL: <http://www.chem.msu.su/cgi-bin/tkv.pl?show=welcome.html>.
52. Veryagin U.D. et al. Thermodynamic Properties of Inorganic Substances: Handbook. Editor Zefirov A.P. Moscow: Atomizdat Publ. 1965. (In Russian).
53. Pankratz L.B., Stuve J.M., Gokcen M.A. Thermodynamic Data for Mineral Technology: Handbook. Bureau of Mines, USA, 1984.
54. Acker J., Bohmhammel K., G.J.K. van den Berg, J.C. van Miltenburg, C. Kloc. Thermodynamic properties of iron silicides FeSi and α-$FeSi_2$. *Journal of Chemical Termodynamics*. 1999, vol. 31, pp. 1523 – 1536.
55. Zaitsev A.I., Zemchenko M.A., Mogutnov B.M. Thermodynamic properties of iron silicides and phase equilibria in (1 - x)Si + xFe}. *Journal of Chemical Termodynamics*. 1991, vol. 23, pp. 933 – 940.
56. Schlesinger M.E. Thermodynamics of Solid Transition-Metal Silicides. *Chemical Reviews*. 1990, vol. 90, no. 4, pp. 607 – 628.
57. Moiseev G.K., Vatolin N.A., Marshuk L.A., Ilyinykh N.I. Temperature Dependencies of the Reduced Gibbs Energy of Some Inorganic Compounds: An ASTRA. OWN Alternative Databank. Yekaterinburg: Ural Branch of RAS, 1997. (In Russian).
58. Gaffet E., Malhouroux N., Abdellaoui M. Far from equilibrium phase transition induced by solid-state reaction in the Fe-Si system. *Journal of Alloys and Compounds*. 1993, vol. 194, pp. 339 – 360.
59. Swintendick A.C. A Theoretical Model for Site Preference of Transition Metal Solutes in Fe_3Si. *Solid State Communications*. 1976, vol. 19, pp. 511 – 515.
60. Chen A-H., Yang X.-M., Lin W.-G. Thermodynamic Equilibrium Analysis on Release Characteristics of Chlorine and Alkali Metals during Combustion of Biomass Residues. *Chinese Journal of Process Engineering*. 2007, vol. 7, no. 5, pp. 989 – 998.
61. Tyurin A.G. Thermodynamics of the Chemical and Electrochemical Stability of

Solid Iron, Chromium, and Nickel Alloys. Chelyabinsk: Publishing House of Chelyabinsk State University, 2011. (In Russian).

62. Tret'yakov Yu. D. Thermodynamics of the Ferrites. Leningrad: Khimiya Publ. 1967. (In Russian).
63. Toropov N.A., Borzakovskiy V.P. Phase Diagrams of Silicate System. Vol. 2. Leningrad: Khimiya Publ. 1965. (In Russian).
64. Handbook of Electrochemistry. Editor Sukhotin A.M. Leningrad: Khimiya Publ. 1981. (In Russian).
65. Cotton F., Wilkinson G. Advanced Inorganic Chemistry. New York – London – Sydney – Toronto: John Wiley & Sons, 1972.
66.. Protsenko V.S. and Danilov F. I. Multistep electrochemical reactions involving transport of intermediates between the near-electrode layer and the bulk solution: A kinetics analysis based on theory of generalized variables (theory of similarity). *Russian Journal of Electrochemistry*. 2005, vol. 41, no. 1, pp. 108 – 112.
67. JANAF Thermochemical Tables. Third Edition. *Journal of Physical and Chemical Reference Data*. 1985, vol. 14. Supplement 1.
68. Charette G.G.,. Flengas S.N. Thermodynamic properties of the oxides of Fe, Ni, Pb, Cu, and Mn, by EMF measurements. *Journal of Electro-chemical Society. Electrochemical Science*. 1968, vol. 115, no. 8, pp. 796 – 804.
69. Navrotsky A. Thermodynamics of Formation of the Silicates and Germanates of some Divalent Transition Metals and of Magnesium. *Journal of Inorganic and Nuclear Chemistry*. 1971, vol. 33, pp. 4035 – 4050.
70. Bassett W.A., Ming L.-C. Disproportionation of Fe_2SiO_4 to $2FeO+SiO_2$ at Pressures up to 250 kbar and Temperatures up to 3000°C. *Physics of the Earth and Planetary Interiors*. 1972, vol. 6, pp. 154 – 160.
71. Jacobs M. H. G., B. H. W. S. de Jong, H. A. J. Oonk. The Gibbs energy formulation of α, γ and liquid Fe_2SiO_4 using Grover, Getting and Kennedy's empirical relation between volume and bulk modulus. *Geochimica et Cosmochimica Acta*. 2001, vol. 65, no. 22, pp. 4231 – 4242.
72. Yong W., Dachs E., Withers A.C., Essene E.J. Heat capacity of γ-Fe_2SiO_4 between 5 and 303 K and derived thermodynamic properties. *Physical Chemistry of Minerals*. 2007, vol. 34, pp. 121 – 127.
73. Bancroft G.M., Maddock A.G., Burns R.G. Application of the Mössbauer effect to silicate mineralogy – I. Iron silicates of known crystal structure. *Geochimica et Cosmochimica Acta*. 1967, vol. 31, pp. 2219 – 2246.
74. Bancroft G.M., Burns R.G., Stone A.J. Application of the Mössbauer effect to silicate mineralogy – II. Iron silicates of unknown and complex crystal structure. *Geochimica et Cosmochimica Acta*. 1968, vol. 32, pp. 547 – 559.
75. Kimyashov A.A., Evtushenko M.V., Shtin S.V., Lykasov A.A. Phase Equilibria in the System Fe – Fe_3O_4 – Fe_2SiO_4 . *Vestnik YUUrGU. Serija Metallurgija*, 2010, vol. 189, no. 13, pp. 10 – 14. (In Russian).
76. Lykasov A.A., Kimyashov A.A. The Conditions of Phase Equilibria in Fe – Si – O System at Temperature Interval of 1100 – 1300 K. *Butlerov Communications*. 2010, vol. 21, no. 7, pp. 42 – 49. (In Russian).
77. Kimyashov A.A. Phase Equilibria in Systems Fe – Al – O and Fe – Si – O at Temperature Interval of 1100 – 1300 K. Dissertation thesis. Chelyabinsk: South Ural State University, 2010.
78. Aplatov A.V., Paderin S.N. Thermodynamic Models of Liquid Multicomponent Metallic Solutions. *Elektrometallurgiya*. 2009, no. 9, pp. 28 – 36. (In Russian).
79. Cramer's Rule – Cramer's Method of solving a system of linear equations. URL: < http://2000clicks.com/mathhelp/MatrixCramersRule.aspx>.

80. Hubbard K.J., Schlom D.G. Thermodynamic stability of binary oxides in contact with silicon. *Journal of Materials Research*. 1996, vol. 11, no. 11, pp. 2757 – 2776.
81. Kiss L. Kinetics of Electrochemical Metal Dissolution. Budapest: Akademiai Kiado, 1988.
82. Pourbaix diagrams / Substances & Technologies. – URL: <http://www.substech.com/dokuwiki/doku.php?id=pourbaix_diagrams>.
83. Eriksson G. An algorithm for the computation of aqueous multicomponent, multiphase equilibria. *Analytica Chimica Acta*. 1979, vol. 112, no. 4, pp. 375 – 383.
84. Nikolaychuk P.A., Tyurin A.G. Thermodynamics of Chemical and Electrochemical Stability of Copper-Nickel Alloys. *Protection of Metals and Physical Chemistry of Surfaces*. 2012, vol. 48, no. 4, pp. 462 – 476.
85. Chemist's Handbook. Editor B. P. Nikol'skii. Moscow: Khimiya, 1964, vol. 3. (In Russian).
86. Ball J.W., Nordstrom D.K. User's manual for WATEQ4F with revised thermodynamic data base and test cases for calculating speciation of major, trace and redox elements in natural waters. US geological survey. Open-file report 91-183. – URL: <http://wwwbrr.cr.usgs.gov/projects/GWC_chemtherm/pubs/wq4fdoc.pdf>.
87. Johnson J.W., Oelkers E.H., Helgeson H.C. SUPCRT92: A software package for calculating the standard molal thermodynamic properties of minerals, gases, aqueous species, and reactions from 1 to 5000 bar and 0 to 1000°C. *Computers & Geosciences*, 1992, vol. 16, no. 7, pp. 899 – 947.
88. Glasby G.P., Schulz H.D. E_H, pH diagrams for Mn, Fe, Co, Ni, Cu and As under seawater conditions: application of two new types of E_H, pH diagrams to the study of specific problems in marine geochemistry. *Aquatic Geochemistry*. 1999, vol. 5, no. 3, pp. 227 – 248.
89. FactSage EpH-Web. – URL: <http://www.sgte.org/ephweb.php>.
90. THERMEXPERT – Potential – pH diagram generator / Argentum Solutions, Inc. – URL: <http://www.argentum solutions. com/cgi-bin/thermexpert>.
91. SUPCRT / Prediction Central. – URL: <http://www.predcent.org/ down load/supcrt.html>.
92. The Geochemist's Workbench (GWB). – Rockware: Earth Science and GIS Software. – URL: <http://www.rockware.com/product/overview.php?id=132>.
93. JNC-TDB. – Japan Nuclear Cycle Organization. URL: <http://migrationdb.jnc.go.jp>.
94. ZZ-HATCHES 19: Database for radiochemical modeling / Nuclear Energy Agency. – URL: <http://www.oecd-nea.org/tools/abstract/detail/nea-1210>.
95. PHREEQC-2: A Computer Program for speciation, batch-reaction, one-dimensional transport, and inverse geochemical calculations / USGS. – URL: <http://wwwbrr.cr.usgs.gov/projects/GWC_coupled/phreeqc>.
96. SOLGASWATER program. – URL: <http://158.227.5.164/Chemical_Diagrams/html/ISP_Solgaswater.htm>.
97. Atlas of Eh-pH diagrams: Intercomparison of thermodynamic databases. Geological survey of Japan. Open file report № 419. National Institute of Advanced Industrial Science and Technology, 2005. – URL: <www.gsj.jp/GDB/openfile/files/no0419/openfile419e.pdf>.
98. Kelsall G.H., Williams R.A.. Electrochemical Behavior of Ferrosilicides (Fe_xSi) in Neutral and Alkaline Aqueous Electrolytes. I. Thermodynamics of Fe-Si-H_2O Systems at 298 K. *Journal of the Electrochemical Society*. 1991, vol. 138, no. 4, pp. 931 – 940.
99. Suzuki T., Akimoto S.-I., Fukai Y. The system iron-enstatite-water at high pressures and temperatures – formation of iron hydride and some geophysical implications. *Physics of the Earth and Planetary Interiors*. 1984, vol. 36, pp. 135 – 144.
100. Yagi T., Hishinuma T. Iron hydride formed by the reaction of iron, silicate,

and water: Implications for the light element of the Earth's core. *Geophysical Research Letters*. 1995, vol. 22, no. 14, pp. 1933 – 1936.

101. Badding J.V., Hemley R.J., Mao H.K. High-Pressure Chemistry of Hydrogen in Metals: In Situ Study of Iron Hydride. *Science*. 1991, vol. 253, pp. 421 – 424.
102. Tkacz M. Thermodynamic properties of iron hydride. *Journal of Alloys and Compounds*. 2002, vol. 330 – 332, pp. 25 – 28.
103. Katsura M. Thermodynamics of nitride and hydride formation by the reaction of metals with flowing NH_3. *Journal of Alloys and Compounds*. 1992, vol. 182, pp. 91 – 102.
104. Sugiyama M., Nakayama T. On Oxide Films of Fe – Si and Fe—Si—Al Alloys at High Temperature. *Journal of the Japanese Institute of Metals*. 1959, vol. 23, pp. 534 – 538.
105. Tuck C.W. Non-protective and Protective Scaling of a Commercial $1^3/_4$ % Alloy in the Range 800ºC – 1000ºC. *Corrosion Science*. 1965, vol. 5, no. 631 – 643.
106. Logani R., Smeltzer W.W. Kinetics of Wustite-Fayalite Scale Formation on Iron-Silicon Alloys. *Oxidation of Metals*. 1969, vol. 1, no. 1, pp. 3 – 21.
107. Logani R.C., Smeltzer W.W. The Development of the Wustite-Fayalite Scale on an Iron-l.5 wt. % Silicon Alloy at 1000ºC. *Oxidation of Metals*. 1971, vol. 3, no. 1, pp. 15 – 32.
108. Logani R.C., Smeltzer W.W. The Growth of Wustite-Fayalite Nodules on an Iron-l.5 wt. % Silicon Alloy Exposed to Carbon Dioxide-Carbon Monoxide Atmospheres. *Oxidation of Metals*. 1971, vol. 3, no. 3, pp. 279 – 290.
109. Svedung I., Vannerberg N.-G. The influence of silicon on the oxidation properties of iron. *Corrosion Science*. 1974, vol. 14, pp. 391 – 399.
110. Moseley P.T., Tappin G., Rivière G.C. The oxidation of Dilute Iron – Silicon Alloys ($[Si] \leq 1 w/o$) in Carbon Dioxide. *Corrosion Science*. 1982, vol. 22, no. 2, pp. 69 – 86.
111. Adachi T., Meier G.H. Oxidation of Iron-Silicon Alloys. *Oxidation of Metals*. 1987, vol. 27, no. 5 – 6, pp. 347 – 366.
112. Ban T., Bohnenkamp K., Engell H.-J. The Formation of Protective Films of Iron – Silicon Alloys. *Corrosion Science*. 1979, vol. 19, pp. 283 – 293.
113. Tyurin A.G., Mosunova T.V., Nikolaychuk P.A. Thermodynamics of Chemical and Electrochemical Stability of Cobalt Silicides. *Vestnik YUUrGU. Serija Khimija*. 2010, vol. 3, no. 11 (187), pp. 52 – 60. (In Russian).
114. Nikolaychuk P.A., Shalyapina T.I., Tyurin A.G., Mosunova T.V. Thermodynamics of Chemical and Electrochemical Stability of Mn – Si System Alloys. *Vestnik YUUrGU. Serija Khimija*. 2010, vol. 4, no. 31 (207), pp. 72 – 82. (In Russian).
115. Nikolaychuk P.A., Tyurin A.G. Thermodynamics of Chemical and Electrochemical Stability of Cu – Si System Alloys. *Butlerov Communications*. 2011, vol. 24, no. 2, pp. 84 – 94. (In Russian).
116. Nikolaychuk P.A., Tyurin A.G. Thermodynamic Assessment of Chemical and Electrochemical Stability of Nickel – Silicon System Alloys. *Corrosion Science*. 2013, vol. 73, pp. 237 – 244.
117. Nikolaychuk P.A., Tyurin A.G. Thermodynamic Evaluation of Corrosion-Electrochemical Behaviour of Silicon Brass CuZn17Si3. *Inorganic Materials*. 2013. vol. 49, no. 5, pp. 457 – 467.
118. Greiner E.S., Marsh J.S., Stoughton B. The Alloys of Iron and Silicon. New York and London: McGraw – Hill Book Company, 1933.
119. Crow W.B., Myers J.R., Jeffreys J.V. Anodic Polarization Behaviour of Fe-Si Alloys in Sulfuric Acid Solutions. *Corrosion*. 1972, vol. 28, no. 3, pp. 77 – 82.
120. Aitov R.G., Shein A.B. The Corrosion – Electrochemical Behaviour of Iron Silicides of Various Compositions in Acids. *Zashchita Metallov- Protection*

of Metals. 1993, vol. 29, no. 6, pp. 895 – 899. (In Russian).

121. R. G. Aitov, A. B. Shein. The Influence of Fluoride-Ions on Anodic Behaviour of Iron, Cobalt and Nickel Silicidesю *Zashchita Metallov- Protection of Metals*. 1994, vol. 30, no. 4, pp. 439 – 440. (In Russian).
122. Shein A.B. and Kanaeva O.V. Anodic Dissolution of the (100) and (110) Faces of Iron Monosilicide in a Sulfuric Acid Electrolyte. *Russian Journal of Electrochemistry*. 2000, vol. 36, no. 8, pp. 913 – 915.
123. Shein A.B. Electrochemical Behaviour of the Eutectic Alloys of Iron, Cobalt and Nickel Silicides and Germanides with Silicon and Germanium. *Zashchita Metallov-Protection of Metals*. 1998, vol. 34, no. 1, pp. 25 – 28. (In Russian).
124. Shein A.B. Effect of the Metal Component on Anodic Dissolvability of Iron, Cobalt and Nickel Silicides. *Zashchita Metallov - Protection of Metals*. 2001, vol. 37, no. 3, pp. 281 – 283. (In Russian).
125. Povroznik V.S. and Shein A.B. Environmental and Inherent Factors That Affect Hydrogen Cathodic Evolution on Silicides of the Iron Family Metals. *Zashchita Metallov - Protection of Metals*. 2007, vol. 43, no. 2, pp. 203 – 207. (In Russian).
126. Shein A.B. Corrosion–Electrochemical Behavior of Iron Family Silicides in Various Electrolytes. *Protection of Metals and Physical Chemistry of Surfaces*. 2010, vol. 46, no. 4, pp. 479 – 488. (In Russian).
127. Kelsall G.H., Williams R.A. Electrochemical Behavior of Ferrosilicides (Fe_xSi) in Neutral and Alkaline Aqueous Electrolytes. II. Fe_xSi Electrochemical Kinetics and Corrosion Behavior. *Journal of the Electrochemical Society*. 1991, vol. 138, no. 4, pp. 941 – 951.
128. Rakityanskaya I.L., Shein A.B. Anodic Behavior of Iron, Cobalt and Nickel Silicides in Alkaline Electrolytes. *Russian Journal of Electrochemistry*. 2006, vol. 42, no. 11, pp. 1208 – 1212.
129. Shein A.B., Rakityanskaya I.L., Lomaeva S.F. Anodic Dissolution of Iron Silicides in Alkaline Electrolyte. *Protection of Metals*. 2007, vol. 43, no. 1, pp. 54 – 58.
130. Omurtag Y., Doruk M. Some Investigations of the Corrosion Characteristics of Fe – Si Alloys. *Corrosion Science*. 1970, vol. 10, pp. 225 – 231.
131. Inoue K. et al. Atomic-Scale Structure and Morphology of Ferric Oxyhydroxides Formed by Corrosion of an Iron–Silicon Alloy. *Materials Transactions*. 2006, vol. 47, no. 2, pp. 243 – 246.
132. Kelsall G.H., Williams R.A. Electrochemical Behavior of Ferrosilicides (Fe_xSi) in Neutral and Alkaline Aqueous Electrolytes. II. The Nature of Passive Films on Fe_xSi Electrodes. *Journal of the Electrochemical Society*. 1991, vol. 138, no. 4, pp. 951 – 957.
133. Suzuki S. et al. *Ex-situ* and *in-situ* X-ray diffractions of corrosion products freshly formed on the surface of an iron–silicon alloy. *Corrosion Science*. 2007, vol. 49, pp. 1081 – 1096.
134. Busse H. et al. Metastable iron silicide phase stabilized by surface segregation on Fe_3Si (100). *Surface Science*. 1997, vol. 381, pp. 133 – 141.
135. Viswanathan A. et al. Formation of WC-iron silicide (Fe_5Si_3) composite clad layer on AISI 316L stainless steel by high power (CO_2) laser. *Surface & Coatings Technology*. 2009, vol. 203, pp. 1618 – 1623.
136. Shimada Y., Kojima H. Magnetic properties of amorphous FeSi thin films. *Journal of Applied Physics*. 1976, vol. 47, no. 9, pp. 4156 – 4159.
137. Motojima S. Vapour-Phase Siliconizing of Iron Plate and Crystal Growth of $FeSi_2$ Using Si_2Cl_6 as a Source of Silicon. *Journal of Crystal Growth*. 1987, vol. 85, pp. 309 – 317.
138. Armijo J.S., Wilde B.E. Influence of Si content on the corrosion resistance of the austenitic Fe – Cr – Ni alloys in

oxidizing acids. *Corrosion Science*. 1968, vol. 8, pp. 649 – 664.

139. Naka M., Hashimoto K., Nasumoto T. Effect of Metalloidal Elements on Corrosion Resistance of Amorphous Iron-Chromium Alloys. *Journal of Non-Crystalline Solids*. 1978, vol. 28, pp. 403 – 413.

140. Rife G. et al. Corrosion of Iron-, Nickel- and Cobalt-base Metallic Glasses Containing Boron and Silicon Metalloids. *Materials Science and Engineering.* 1981, vol. 48, pp. 73 – 79.

ТЕРМОДИНАМИЧЕСКАЯ ОЦЕНКА ХИМИЧЕСКОЙ И ЭЛЕКТРОХИМИЧЕСКОЙ УСТОЙЧИВОСТИ СИЛИЦИДОВ ЖЕЛЕЗА

П.А. Николайчук

Институт биохимии, Грайфсвальдский университет,
Ул. имени Феликса Хаусдорфа 4, 17487 Грайфсвальд, Германия.
e-mail: npa@csu.ru.

Рассмотрены фазовые и химические равновесия в системе Fe – Si при 298 K. Произведено сравнение имеющейся в наличии термодинамической информации о растворимости кремния в железе с решёткой о. ц. к. при низких температурах с учётом и без учёта дальнего упорядочения в α-фазе. Оценена стандартная энергия Гиббса образования нестехиометричного силицида железа. Оценена возможная максимальная растворимость кремния в железе при 298 K и вычислены термодинамические активности насыщенного раствора. Построена диаграмма состояния системы Fe – Si – O при 298 K и вычислены характеристик инвариантных состояний этой системы. Оценена твёрдая растворимость Fe_2SiO_4 в Fe_3O_4 и SiO_2 в Fe_2O_3 при 298 K. Построены диаграммы активность – pH для соединений железа (II) и железа (III) в водных средах. Построена диаграмма потенциал – pH системы Fe – Si – H_2O при 298 K, давлении воздуха 1 бар и активностях ионов в растворе, равных 1 моль/л. Рассмотрены основные химические и электрохимические равновесия в системе. Выполнен термодинамический анализ химической и электрохимической устойчивости сплавов системы Fe – Si.
***Ключевые слова**: система Fe–Si, силициды железа, фазовые равновесия, низкотемпературное окисление, химическая и электрохимическая устойчивость.*

DƏMİR SİLİSİDLƏRİN KİMYƏVİ VƏ ELEKTROKİMYƏVİ DAYANIQLIĞININ TERMODİNAMİKİ QİYMƏTLƏNDİRİLMƏSİ

P.A. Nikolayçuk

Qrayfsvald Universiteti, Biokimya İnstitutu, Almaniya
17487 Qrayfsvald, Almaniya, Feliks Hausdorf küç.,4; e-mail: npa@csu.ru

Fe – Si sistemində 298K temperaturda faza və kimyəvi tarazlıqlar nəzərdən keçirilib. Silisiumun dəmirdə aşağı temperaturda həll olması haqqında ədəbiyyatda olan informasiya müqayisə edilib və əmələ gələn doymuş məhlulun termodinamik aktivliyi hesablanıb. Fe – Si sistemin kimyəvi və elektrokimyəvi dayanıqlığının termodinamiki analizi aparılıb.
***Açar sözlər:** Fe – Si sistemi, faza tarazlığı, kimyəvi və elektrokimyəvi dayanıqlıq*